Mechanics of Materials 185 (2023) 104751

Contents lists available at ScienceDirect

Mechanics of Materials

journal homepage: www.elsevier.com/locate/mecmat

Editor invited article

Configurational peridynamics

P. Steinmann [a,b], A.M. de Villiers [c,*], A.T. McBride [b], A. Javili [d]

[a] Institute of Applied Mechanics, University of Erlangen–Nuremberg, Egerlandstr. 5, 91058 Erlangen, Germany
[b] Glasgow Computational Engineering Centre, School of Engineering, University of Glasgow, Glasgow G12 8QQ, United Kingdom
[c] Applied Mathematics, Stellenbosch University, Private Bag X1., Matieland, 7602, South Africa
[d] Department of Mechanical Engineering, Bilkent University, 06800 Ankara, Turkey

ARTICLE INFO

Keywords:
Peridynamics
Configurational mechanics
Nonlocal mechanics
Nonlinear kinematics

ABSTRACT

Configurational forces that drive the evolution of material structures such as defects are introduced into a geometrically-exact peridynamics framework. The concept of bond-number double-density facilitates the definition of a peridynamic potential energy functional that inherits the key features of its conventional (local) continuum and discrete counterparts. The spatial and material variations of the peridynamic potential energy functional give rise to familiar Piola- and Cauchy-type bond-wise interaction forces that enter the point-wise force balance in the spatial and material setting, respectively. It is shown that the point-wise material body force density is a result of a non-local pull-back of the bond-wise spatial interaction force, and thereby captures non-local contributions. Several key features of configurational peridynamics are demonstrated via a computational example and a comparison to conventional configurational continuum mechanics.

1. Introduction

Configurational mechanics provides a framework for understanding the behaviour of defects and quantifying the energy release due to changes of the material configuration. Peridynamics (PD) is a non-local continuum formulation that inherently allows for such defects and is widely used for modelling fracture and damage. The primary objective of this work is to combine these two complementary approaches and detail a configurational mechanics framework for peridynamics.

The standard familiar forces in continuum mechanics arise in response to the motion of continuum points. The less familiar configurational forces arise due to the response of a continuum body to variations in the material (reference) placement of its points. Configurational forces drive the internal restructuring of material and are basic objects consistent with their own force balance. They are necessary to present a comprehensive picture of a body's reaction to the evolution of defects (Podio-Guidugli, 2002). Configurational mechanics is therefore ideally suited to describe the role of defects such as dislocations, inhomogeneities, inclusions, interfaces and cracks, (see, e.g. Gurtin and Podio-Guidugli, 1996a, 1998; Fried and Gurtin, 2003) and the collection by Steinmann and Maugin (2006). The unifying notion of configurational mechanics encompasses all forms of driving "forces" on such defects including both smooth and abrupt inhomogeneities in fracture mechanics (Maugin, 1995; Näser et al., 2007; Kuhn and Müller, 2016). Configurational mechanics has also been applied to model and analyse other phenomena such as growth (Fried and Gurtin, 2003), rate-dependent materials (Cermelli et al., 2001; Svendsen et al., 2009) and the complex motion of highly elastic constrained rods (Bosi et al., 2016; Liakou and Detournay, 2018; Armanini et al., 2019). The theoretical underpinnings of configurational mechanics have been developed over the last half-century beginning with the seminal work by Eshelby (1951, 1975) and important contributions by Gurtin (1995), Gurtin and Podio-Guidugli (1996b), Kienzler and Herrmann (2000), Maugin (2016, 2020), Cermelli and Fried (1997), among others. Our own contributions include Steinmann (2002a,b,c, 2008), Steinmann et al. (2012). For a comprehensive overview, see Gurtin (2000), Maugin (2016, 2020), Steinmann (2022).

PD (Silling, 2000) is a non-local formulation of continuum mechanics - a subset of generalised continuum formulations (Cordero et al., 2016; Forest, 2009; Dillard et al., 2006) - in which the behaviour of a continuum point is influenced by interactions with other points within a finite *horizon*. As such, PD inherits many features of atomistic approaches. According to Dell'Isola et al. (2015), the roots of PD may be traced back to the pioneering works of Piola. Due to the integral form of the governing equations, PD is particularly well suited for problems with discontinuities and has thus been predominantly employed to model material failure and fracture (see, e.g. Silling et al., 2010; Ha

Invited Editor: Laura De Lorenzis.

* Corresponding author.
E-mail addresses: paul.steinmann@fau.de (P. Steinmann), andiedevilliers@sun.ac.za (A.M. de Villiers), Andrew.McBride@glasgow.ac.uk (A.T. McBride), ajavili@bilkent.edu.tr (A. Javili).

https://doi.org/10.1016/j.mechmat.2023.104751
Received 20 March 2023; Received in revised form 24 July 2023; Accepted 25 July 2023
Available online 31 July 2023

and Bobaru, 2011; Silling and Askari, 2005; Bobaru and Zhang, 2015; Ebrahimi et al., 2015; Butt and Meschke, 2021; Dorduncu and Madenci, 2022). For an extensive overview of PD theory, applications and related studies, see the review by Javili et al. (2019b).

Despite the substantial body of work on PD and fracture propagation, the handling of crack initiation and subsequent propagation in PD is controlled by a constitutive prescription requiring the bond-wise interaction forces to eventually vanish as bond elongation increases. We argue here that in a continuum body (i) initiation of a true crack must be accompanied by a change in the topology that describes the geometry of the body, and (ii) true fracture propagation is irreversible and results in energy dissipation inside the body or energy release from the body. Configurational mechanics provides the correct tool to address these key characteristics of both initiation and propagation of fracture. However, the notion of configurational forces is entirely absent in all contributions pertaining to PD to date. Via rigorous mathematical derivations, this contribution addresses this shortcoming and lays the groundwork for a configurational peridynamics framework. Furthermore, the key features and insights that our framework provides are elucidated through a series of computational simulations highlighting the utility and enormous potential of the formulation.

This manuscript is organised as follows. To set the stage and introduce the notation, a brief recap of configurational mechanics is given in Section 2. Continuous systems are addressed first, followed by their atomistic counterparts. These provide the necessary foundations for the primary contribution of the manuscript in Section 3 wherein the configurational peridynamics framework is presented. Section 4 elucidates the developed theory through a series of numerical examples in two dimensions together with comparisons with classical continuum mechanics solved using the finite element method. Section 5 concludes this work, summarises our important findings and provides an outlook.

2. Brief recap of configurational mechanics

Deformational mechanics is concerned with the response of a mechanical system to externally applied loading. Its aim is to determine the resulting spatial position into which each point (discrete or continuous) is mapped from its original material placement. If the potential energy is expressed as a functional of the spatial positions of the points, and the system is subjected to spatial variations, i.e., variations of the spatial positions, the Euler–Lagrange equations (or localised force balance) are obtained from the stationary point of the potential energy functional. By contrast, *configurational mechanics* is concerned with the energetic changes associated with a variation of the material configuration. When the total potential energy is expressed as a functional of the material position of points, the material variation thereof does not generally have a stationary point but rather defines a change in, or more specifically a release of, potential energy. This energy is available to drive other physical processes such as the creation of crack surfaces. This section begins with a brief recap of configurational mechanics. As (configurational) PD borrows ideas from both continuum and molecular mechanics, the relevant ideas from these perspectives are also emphasised.

2.1. Continuous systems: The case of hyperelastic continuum mechanics

First the terminology describing the relevant kinematic quantities of a continuum body are reviewed. This is followed by spatial and material variations of the potential energy functional which lead to the deformational equilibrium equations when a spatial variation is considered and the configurational non-equilibrium equations, defining potential energy release upon a configurational change, when a material variation is considered. The configurational non-equilibrium equations provide an expression for the potential energy release in terms of material tractions at boundaries (and interfaces).

2.1.1. Kinematics

As depicted in Fig. 1, the motion of a continuum body that initially occupies the material configuration $\mathcal{B}_0$ and deforms as it is subjected to a prescribed external loading into the spatial configuration $\mathcal{B}_t$ is described in terms of the material and spatial placements, $\boldsymbol{X}$ and $\boldsymbol{x}$, respectively. These are related by the spatial deformation map as $\boldsymbol{x} = \boldsymbol{y}(\boldsymbol{X})$. The tangent map between infinitesimal line elements $\mathrm{d}\boldsymbol{X}$ and $\mathrm{d}\boldsymbol{x}$ in the material and spatial configuration, i.e., the deformation gradient, is given by $\boldsymbol{F} = \nabla_{\boldsymbol{X}}\boldsymbol{y}$, where the gradient operator $\nabla_{\boldsymbol{X}}$ is with respect to the material coordinates. The deformation can be described from an alternative perspective by using the material deformation map $\boldsymbol{X} = \boldsymbol{Y}(\boldsymbol{x})$, where $\boldsymbol{Y} = \boldsymbol{y}^{-1}$ denotes the inverse functional relation between $\boldsymbol{X}$ and $\boldsymbol{x}$, and its associated tangent map $\boldsymbol{f} = \nabla_{\boldsymbol{x}}\boldsymbol{Y}$, where $\boldsymbol{f} = \boldsymbol{F}^{-1}$ is the algebraic inverse of $\boldsymbol{F}$. Note, we omit the more precise notation $\boldsymbol{f} = \boldsymbol{F}^{-1}\circ\boldsymbol{Y}(\boldsymbol{x})$ for the sake of conciseness as well as the explicit indication of the parameterisation if there is no danger of confusion. The spatial area map $\boldsymbol{K} = \mathrm{cof}\boldsymbol{F}$, also known as the cofactor, maps infinitesimal area elements $\mathrm{d}\boldsymbol{A}$ and $\mathrm{d}\boldsymbol{a}$ in the material and spatial configuration with the inverse relation given by the material area map $\boldsymbol{k} = \mathrm{cof}\boldsymbol{f}$. Finally, the spatial volume map $J = \det\boldsymbol{F}$, also known as the Jacobian determinant, maps the infinitesimal volume element $\mathrm{d}V$ in the material configuration into its counterpart $\mathrm{d}v$ in the spatial configuration. Likewise, the material volume map $j = J^{-1}$ gives the volume ratio between infinitesimal volume elements in the material and spatial configurations.

In summary, the transformations for the various infinitesimal line, area and volume elements are

$$\begin{aligned}
&\mathrm{d}\boldsymbol{x} = \boldsymbol{F}\cdot\mathrm{d}\boldsymbol{X} \quad \text{with} \quad \boldsymbol{F} = \nabla_{\boldsymbol{X}}\boldsymbol{y}\,; \quad \mathrm{d}\boldsymbol{X} = \boldsymbol{f}\cdot\mathrm{d}\boldsymbol{x} \quad \text{with} \quad \boldsymbol{f} = \nabla_{\boldsymbol{x}}\boldsymbol{Y}\,,\\
&\mathrm{d}\boldsymbol{a} = \boldsymbol{K}\cdot\mathrm{d}\boldsymbol{A} \quad \text{with} \quad \boldsymbol{K} = \mathrm{cof}\boldsymbol{F}\,; \quad \mathrm{d}\boldsymbol{A} = \boldsymbol{k}\cdot\mathrm{d}\boldsymbol{a} \quad \text{with} \quad \boldsymbol{k} = \mathrm{cof}\boldsymbol{f}\,,\\
&\mathrm{d}v = J\,\mathrm{d}V \quad \text{with} \quad J = \det\boldsymbol{F}\,; \quad \mathrm{d}V = j\,\mathrm{d}v \quad \text{with} \quad j = \det\boldsymbol{f}\,.
\end{aligned} \tag{1}$$

2.1.2. Potential energy functional and its spatial and material variations

The potential energy functional I can be expressed as the integral of the potential energy density per volume over the body in either parameterisation $I = I(\boldsymbol{y};\boldsymbol{X})$ or $I = I(\boldsymbol{Y};\boldsymbol{x})$ by interchanging the fields and parameterisation, that is

$$I(\boldsymbol{y};\boldsymbol{X}) = \int_{\mathcal{B}_0} U_0(\boldsymbol{y},\boldsymbol{F};\boldsymbol{X})\,\mathrm{d}V \quad \text{or} \quad I(\boldsymbol{Y};\boldsymbol{x}) = \int_{\mathcal{B}_t} U_t(\boldsymbol{Y},\boldsymbol{f};\boldsymbol{x})\,\mathrm{d}v\,. \tag{2}$$

Here the semicolon distinguishes functional dependence from parameterisation. More precisely, $I(\boldsymbol{y};\boldsymbol{X})$ denotes that I depends on $\boldsymbol{y}(\boldsymbol{X})$ and is parameterised in $\boldsymbol{X}$. The potential energy density U_0 per unit volume in the material configuration and U_t per unit volume in the spatial configuration most generally consist of internal and external contributions and are related by the Jacobian determinants as $U_0 = JU_t$ and $U_t = jU_0$. For the sake of presentation, all boundary contributions are neglected.

Remark 1. A *spatial variation* D_δ of the potential energy functional $I(\boldsymbol{y};\boldsymbol{X})$ in Eq. $(2)_a$ considers perturbations of the spatial deformation map $\boldsymbol{y}(\boldsymbol{X})$ in terms of admissible spatial variations $\mathrm{D}_\delta\boldsymbol{y}(\boldsymbol{X})$ at fixed material placements $\boldsymbol{X}$, that is

$$\mathrm{D}_\delta I(\boldsymbol{y}(\boldsymbol{X});\boldsymbol{X}) = \frac{\mathrm{d}}{\mathrm{d}\epsilon} I\big(\boldsymbol{y}(\boldsymbol{X}) + \epsilon\,\mathrm{D}_\delta\boldsymbol{y}(\boldsymbol{X});\boldsymbol{X}\big)\Big|_{\epsilon=0} = \delta I\Big|_{\boldsymbol{X}}\,. \tag{3}$$

Likewise, a *material variation* d_δ of the potential energy functional $I(\boldsymbol{Y};\boldsymbol{x})$ in Eq. $(2)_b$ considers perturbations of the material deformation map $\boldsymbol{Y}(\boldsymbol{x})$ in terms of admissible material variations $\mathrm{d}_\delta\boldsymbol{Y}(\boldsymbol{x})$ at fixed spatial placements $\boldsymbol{x}$ as follows

$$\mathrm{d}_\delta I(\boldsymbol{Y}(\boldsymbol{x});\boldsymbol{x}) = \frac{\mathrm{d}}{\mathrm{d}\epsilon} I\big(\boldsymbol{Y}(\boldsymbol{x}) + \epsilon\,\mathrm{d}_\delta\boldsymbol{Y}(\boldsymbol{x});\boldsymbol{x}\big)\Big|_{\epsilon=0} = \delta I\Big|_{\boldsymbol{x}}\,. \tag{4}$$

Admissible spatial and material variations respect the corresponding Dirichlet boundary conditions. □

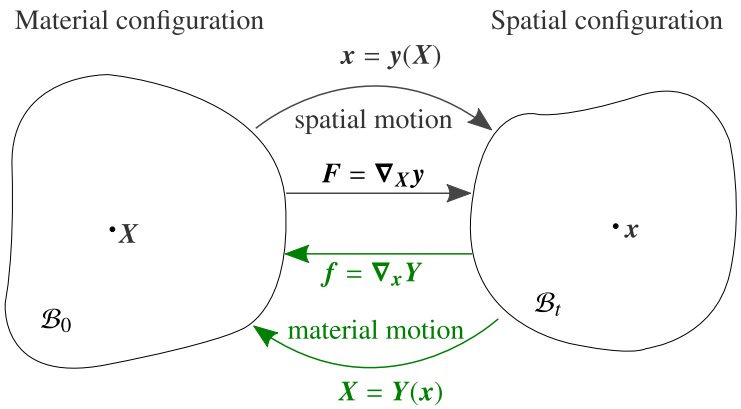

Fig. 1. Spatial and material motion of a continuum body.

Spatial variations, i.e., variations at fixed material placement, of the potential energy functional $I(\boldsymbol{y};\boldsymbol{X})$ render the stationary point $\mathrm{D}_\delta I(\boldsymbol{y};\boldsymbol{X}) \doteq 0$ as

$$\begin{aligned}\mathrm{D}_\delta I(\boldsymbol{y};\boldsymbol{X}) &= \int_{\mathcal{B}_0} \left[\partial_{\boldsymbol{F}} U_0 : \nabla_{\boldsymbol{X}} \mathbf{D}_\delta \boldsymbol{y} + \partial_{\boldsymbol{y}} U_0 \cdot \mathrm{D}_\delta \boldsymbol{y}\right] \mathrm{d}V \\ &=: \int_{\mathcal{B}_0} \left[\boldsymbol{P} : \nabla_{\boldsymbol{X}} \mathbf{D}_\delta \boldsymbol{y} - \boldsymbol{b}_0 \cdot \mathrm{D}_\delta \boldsymbol{y}\right] \mathrm{d}V \\ &= \int_{\mathcal{B}_t} \left[\boldsymbol{\sigma} : \nabla_{\boldsymbol{x}} \mathbf{D}_\delta \boldsymbol{y} - \boldsymbol{b}_t \cdot \mathbf{D}_\delta \boldsymbol{y}\right] \mathrm{d}v \doteq 0\,,\end{aligned} \tag{5}$$

and results in the localised force balances (or deformational equilibrium statements) as the corresponding Euler–Lagrange equations:

$$\mathrm{Div}\boldsymbol{P} + \boldsymbol{b}_0 = \boldsymbol{0} \qquad \text{and} \qquad \mathrm{div}\boldsymbol{\sigma} + \boldsymbol{b}_t = \boldsymbol{0}\,. \tag{6}$$

Here $\boldsymbol{P}$ is the (two-point) Piola stress tensor and $\boldsymbol{\sigma}$ is the (spatial) Cauchy stress tensor. These are related by Piola transforms as $\boldsymbol{P} = \boldsymbol{\sigma}\cdot\boldsymbol{K}$ and $\boldsymbol{\sigma} = \boldsymbol{P}\cdot\boldsymbol{k}$, respectively. The vectors $\boldsymbol{b}_0$ and $\boldsymbol{b}_t$ denote the spatial body force per unit volume in the material and spatial configurations, respectively.

Alternatively, if the potential energy functional $I(\boldsymbol{Y};\boldsymbol{x})$ is parameterised in $\boldsymbol{x}$ as in $(2)_b$, its material variation $\mathrm{d}_\delta I$, i.e., a variation at fixed spatial placement, can be considered. However, excluding rare instances of configurational equilibrium, $\mathrm{d}_\delta I$ does not render a stationary point but rather defines a change, or more specifically (in accordance with the second law of thermodynamics) a release of potential energy $\mathcal{R} \le 0$. That is

$$\begin{aligned}\mathrm{d}_\delta I(\boldsymbol{Y};\boldsymbol{x}) &= \int_{\mathcal{B}_t} \left[\partial_{\boldsymbol{f}} U_t : \nabla_{\boldsymbol{x}} \mathbf{d}_\delta \boldsymbol{Y} + \partial_{\boldsymbol{Y}} U_t \cdot \mathrm{d}_\delta \boldsymbol{Y}\right] \mathrm{d}v \\ &=: \int_{\mathcal{B}_t} \left[\boldsymbol{p} : \nabla_{\boldsymbol{x}} \mathbf{d}_\delta \boldsymbol{Y} - \boldsymbol{B}_t \cdot \mathrm{d}_\delta \boldsymbol{Y}\right] \mathrm{d}v \\ &= \int_{\mathcal{B}_0} \left[\boldsymbol{\Sigma} : \nabla_{\boldsymbol{X}} \mathbf{d}_\delta \boldsymbol{Y} - \boldsymbol{B}_0 \cdot \mathrm{d}_\delta \boldsymbol{Y}\right] \mathrm{d}V =: \mathcal{R} \le 0.\end{aligned} \tag{7}$$

Here $\boldsymbol{p}$ is a two-point Piola-type stress tensor associated with the material variation of the potential energy density U_t and $\boldsymbol{\Sigma}$ is the celebrated (material) Eshelby stress tensor. These quantities are related by Piola transforms as $\boldsymbol{p} = \boldsymbol{\Sigma}\cdot\boldsymbol{k}$ and $\boldsymbol{\Sigma} = \boldsymbol{p}\cdot\boldsymbol{K}$, respectively. The vectors $\boldsymbol{B}_t$ and $\boldsymbol{B}_0$ denote the material body force (material inhomogeneity force in the terminology of Maugin (1995)) per unit volume in the spatial and material configurations, respectively. Material inhomogeneities are accounted for via the explicit dependence of the potential energy density on the material position $\boldsymbol{X} = \boldsymbol{Y}(\boldsymbol{x})$. Applying integration by parts and the divergence theorem renders the expression for the energy release as

$$\mathcal{R} = \int_{\partial\mathcal{B}_0} \left[\boldsymbol{\Sigma}\cdot\boldsymbol{N}\right] \cdot \mathbf{d}_\delta \boldsymbol{Y}\,\mathrm{d}A - \int_{\mathcal{B}_0} \underbrace{\left[\mathrm{Div}\boldsymbol{\Sigma} + \boldsymbol{B}_0\right]}_{=\boldsymbol{0}\ (\text{see } §2.1.3)} \cdot \mathbf{d}_\delta \boldsymbol{Y}\,\mathrm{d}V \le 0\,. \tag{8}$$

Before analysing this expression further in order to emphasise the role of the Eshelby stress in the energy release, it proves helpful to uncover how the spatial and material localised force balances are related in the bulk.

2.1.3. Relating spatial and material localised force balances in the bulk

It is interesting to note that the (material) Eshelby stress as well as the (spatial) Cauchy stress can be written in the so-called energy–momentum format as follows

$$\boldsymbol{\Sigma} = U_0\boldsymbol{I} - \boldsymbol{F}^{\mathrm{t}}\cdot\boldsymbol{P} \qquad \text{and} \qquad \boldsymbol{\sigma} = U_t\boldsymbol{i} - \boldsymbol{f}^{\mathrm{t}}\cdot\boldsymbol{p}\,. \tag{9}$$

These relations follow immediately from the product and chain rules of differentiation.

Pre-multiplying the spatial localised force balance in (6) (deformational equilibrium) $\mathrm{Div}\boldsymbol{P} + \boldsymbol{b}_0 = \boldsymbol{0}$ with $-\boldsymbol{F}^{\mathrm{t}}$ and accounting for the various dependencies of the potential energy density $U_0(\boldsymbol{y},\boldsymbol{F};\boldsymbol{X})$, the localised force balance can alternatively be expressed as $\mathrm{Div}\boldsymbol{\Sigma} + \boldsymbol{B}_0 = \boldsymbol{0}$, i.e., in terms of the Eshelby stress $\boldsymbol{\Sigma}$ (see Eq. (8)). From the Piola transformation $\boldsymbol{p} = \boldsymbol{\Sigma}\cdot\boldsymbol{k}$, the localised force balance can also be expressed in terms of the material Piola-type stress $\boldsymbol{p} = \partial_{\boldsymbol{f}} U_t$. Fig. 2 illustrates the four equivalent localised force balances and highlights the direct relationship between them. As an interpretation, in the bulk, all localised force balances in Fig. 2 express the same physical statement of equilibrium since they are simply related by pull back and push forward operations in terms of the transposed deformations gradients. Using these relations, the energy release in Eq. (8) reduces to

$$\mathcal{R} = \int_{\partial\mathcal{B}_0} \left[\boldsymbol{\Sigma}\cdot\boldsymbol{N}\right] \cdot \mathbf{d}_\delta \boldsymbol{Y}\,\mathrm{d}A \le 0\,. \tag{10}$$

It is thus clear that the energy release is due to the material or Eshelby traction $\boldsymbol{T}_0 := \boldsymbol{\Sigma}\cdot\boldsymbol{N}$ expressed in terms of the normal projection of the Eshelby stress. Taken together, the material traction $\boldsymbol{T}_0$ is power conjugated to virtual material (configurational) changes $\mathrm{d}_\delta\boldsymbol{Y}$ of the boundary $\partial\mathcal{B}_0$.

2.1.4. Energy release at a crack tip

At a crack tip, the corresponding contribution to the energy release $\mathcal{R}_{\mathrm{crack}}$ can be determined from Eq. (10) by considering the boundary of an *isolated* ball $\mathscr{B}_0$ with radius r_0 centred at the crack tip singularity, see Fig. 3. Thus,

$$\begin{aligned}\mathcal{R}_{\mathrm{crack}} &= \lim_{r_0\to 0} \int_{\partial\mathscr{B}_0} \left[\boldsymbol{\Sigma}\cdot\boldsymbol{N}\right] \cdot \mathrm{d}_\delta \boldsymbol{Y}\,\mathrm{d}A =: -\boldsymbol{J}\cdot\mathrm{d}_\delta\boldsymbol{Y}\Big|_{r_0\to 0} \le 0 \qquad \text{with} \\ \boldsymbol{J} &:= -\lim_{r_0\to 0} \int_{\partial\mathscr{B}_0} \boldsymbol{\Sigma}\cdot\boldsymbol{N}\,\mathrm{d}A\,.\end{aligned} \tag{11}$$

Here $\boldsymbol{J}$ coincides with the vectorial version of the celebrated J-integral in classical fracture mechanics. The negative sign is present as $\boldsymbol{J}$ is usually written in terms of the normal pointing towards the outside

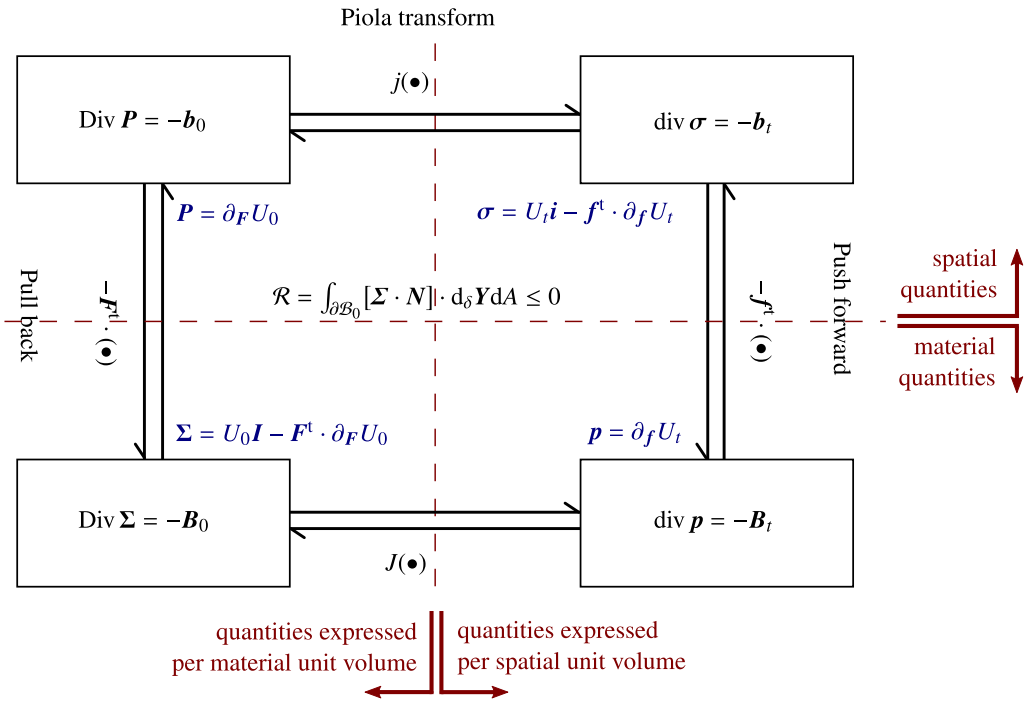

Fig. 2. Transformations between equivalent localised force balances.

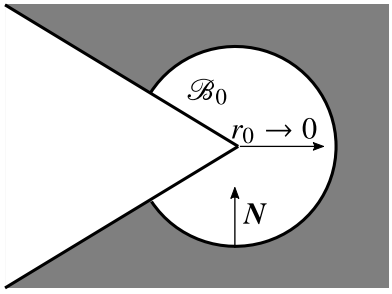

Fig. 3. The energy available for release due to a crack tip singularity is considered by cutting out a ball $\mathcal{B}_0$ with radius r_0 and letting it shrink to zero. Note the orientation of the normal pointing towards the crack tip.

of $\mathcal{B}_0$, i.e., away from the crack tip and towards the inside of the body $\mathcal{B}_0$.

2.2. Discrete systems: The case of bond-based atomistics

In the following section, the concepts of deformational (and configurational) equilibrium and energy release are detailed for a system of discrete interacting atoms. For the sake of representation, only bond-wise interactions are considered, see Steinmann et al. (2011) for further details. For multibody interactions, see Steinmann et al. (2021).

2.2.1. Kinematics

Consider a discrete atomwise-motion of a system that contains a finite number of atoms listed in the set $\mathcal{I}_C$ (see Fig. 4). We consider the quasi-static case, wherein the sequence of events due to quasi-static loading is ordered by a time-like variable s and we distinguish between (discrete) material and spatial configurations $\mathcal{C}_0$ and $\mathcal{C}_t$, respectively. These two configurations are defined by the sets containing the position of each atom α in $\mathcal{I}_C$, collectively denoted by $\{\boldsymbol{X}^\alpha\} = \{\boldsymbol{x}^\alpha(0)\}$ and $\{\boldsymbol{x}^\alpha\} = \{\boldsymbol{x}^\alpha(s)\}$, respectively, with $\alpha = 1, 2, 3, \dots, n_{\text{atom}}$. Note that n_{atom} may be very large but finite. The set $\mathcal{I}_{\mathcal{N}^\alpha}$ lists the neighbouring atoms for each atom α that are within a given cut-off radius δ_0. To emphasise the different perspectives of deformational and configurational mechanics, a spatial motion of atom α is described in terms of its material placement $\boldsymbol{X}^\alpha$ and its spatial position $\boldsymbol{y}^\alpha$ while a material motion of atom α is described in terms of its spatial placement $\boldsymbol{x}^\alpha$ and its material position $\boldsymbol{Y}^\alpha$.

The bond vectors between pairs of atoms characterise the system further as the distance between two atoms, or the bond length, contributes to the potential energy. The bond vectors are expressed in terms of the bond length and bond directions as

$$\begin{aligned}
\boldsymbol{\Xi}^{\alpha\beta} &:= \boldsymbol{X}^\beta - \boldsymbol{X}^\alpha = |\boldsymbol{X}^\beta - \boldsymbol{X}^\alpha| \boldsymbol{E}^{\alpha\beta} = \Xi^{\alpha\beta} \boldsymbol{E}^{\alpha\beta}, \\
\boldsymbol{\xi}^{\alpha\beta} &:= \boldsymbol{x}^\beta - \boldsymbol{x}^\alpha = |\boldsymbol{x}^\beta - \boldsymbol{x}^\alpha| \boldsymbol{e}^{\alpha\beta} = \xi^{\alpha\beta} \boldsymbol{e}^{\alpha\beta}, \\
\boldsymbol{Y}^{\alpha\beta} &:= \boldsymbol{Y}^\beta - \boldsymbol{Y}^\alpha = |\boldsymbol{Y}^\beta - \boldsymbol{Y}^\alpha| \boldsymbol{E}^{\alpha\beta} = Y^{\alpha\beta} \boldsymbol{E}^{\alpha\beta}, \\
\boldsymbol{\upsilon}^{\alpha\beta} &:= \boldsymbol{y}^\beta - \boldsymbol{y}^\alpha = |\boldsymbol{y}^\beta - \boldsymbol{y}^\alpha| \boldsymbol{e}^{\alpha\beta} = \upsilon^{\alpha\beta} \boldsymbol{e}^{\alpha\beta}.
\end{aligned} \tag{12}$$

Here, a distinction is made between bond vectors, together with their associated length and direction, based on either the material and spatial placements $\boldsymbol{\Xi}^{\alpha\beta}$ and $\boldsymbol{\xi}^{\alpha\beta}$, or the material and spatial positions $\boldsymbol{Y}^{\alpha\beta}$ and $\boldsymbol{\upsilon}^{\alpha\beta}$, respectively. Key deformation measures are then the bond stretches

$$\lambda^{\alpha\beta} := \upsilon^{\alpha\beta} / \Xi^{\alpha\beta} \qquad \text{and} \qquad \Lambda^{\alpha\beta} := Y^{\alpha\beta} / \xi^{\alpha\beta}, \tag{13}$$

corresponding to the spatial and material motion, respectively.

2.2.2. Potential energy functional and its spatial and material variations

The potential energy functional I can be expressed as the summation of the potential energy contributions over all the atoms in the system (following ideas similar to Fried (2010)) in either parameterisation $I = I(\{\boldsymbol{y}^\epsilon\}; \{\boldsymbol{X}^\epsilon\})$ or $I = I(\{\boldsymbol{Y}^\epsilon\}; \{\boldsymbol{x}^\epsilon\})$ by interchanging the fields and parameterisation, that is

$$\begin{aligned}
I(\{\boldsymbol{y}^\epsilon\}; \{\boldsymbol{X}^\epsilon\}) &= \frac{1}{2} \sum_{\alpha \in \mathcal{I}_C} \sum_{\beta \in \mathcal{I}_{\mathcal{N}^\alpha}} W_0^{\alpha\beta}(\lambda^{\alpha\beta}) \Xi^{\alpha\beta} \qquad \text{or} \\
I(\{\boldsymbol{Y}^\epsilon\}; \{\boldsymbol{x}^\epsilon\}) &= \frac{1}{2} \sum_{\alpha \in \mathcal{I}_C} \sum_{\beta \in \mathcal{I}_{\mathcal{N}^\alpha}} W_t^{\alpha\beta}(\Lambda^{\alpha\beta}) \xi^{\alpha\beta}.
\end{aligned} \tag{14}$$

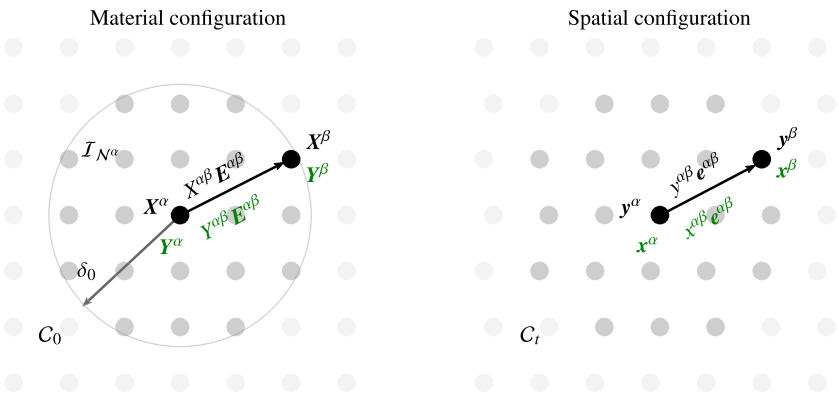

Fig. 4. Material and spatial configurations for an atomistic system. A spatial motion is described in terms of $\boldsymbol{X}^\alpha$ and $\boldsymbol{y}^\alpha$ and a material motion in terms of $\boldsymbol{x}^\alpha$ and $\boldsymbol{Y}^\alpha$ with $\alpha = 1, 2, 3, \dots, n_{\text{atom}}$.

The spatial and material internal bond potentials between two atoms, denoted $W_0^{\alpha\beta}$ and $W_t^{\alpha\beta}$ respectively, are expressed in terms of their density per unit bond length in the material and spatial configurations, respectively. Consequently, the bond potentials are related as $W_0^{\alpha\beta} = W_t^{\alpha\beta}\lambda^{\alpha\beta}$ and $W_t^{\alpha\beta} = W_0^{\alpha\beta}\Lambda^{\alpha\beta}$. Note that, without loss of generality, these potentials are parameterised by the bond stretches $\lambda^{\alpha\beta}$ and $\Lambda^{\alpha\beta}$ and not the bond lengths as is standard in atomistic treatments. Any external potential energy contributions related to the atoms are neglected here for the sake of presentation. The energy contribution of a particular atom α is due to the *summation* of all the bond potentials in $\mathcal{I}_{\mathcal{N}^\alpha}$, i.e., within the cut-off, and is numerically the same regardless of the perspective adopted, that is

$$\sum_{\beta\in\mathcal{I}_{\mathcal{N}^\alpha}} W_0^{\alpha\beta}\,\Xi^{\alpha\beta} = \sum_{\beta\in\mathcal{I}_{\mathcal{N}^\alpha}} W_t^{\alpha\beta}\,\xi^{\alpha\beta}\,. \tag{15}$$

Note that the summation over a discrete number of atoms α in a discrete atomistic system replaces the notion of integration over a point-wise potential energy density in a continuous system. Summation over the neighbouring atoms β in $\mathcal{I}_{\mathcal{N}^\alpha}$ may be considered as an expression of *nonlocality* naturally inherent to atomistic systems.

Following the same arguments as in the preceding section, spatial variations of the potential energy functional $I(\{\boldsymbol{y}^\epsilon\};\{\boldsymbol{X}^\epsilon\})$ in Eq. $(14)_a$ render the stationary point $\mathrm{D}_\delta I(\{\boldsymbol{y}^\epsilon\};\{\boldsymbol{X}^\epsilon\}) \doteq 0$ as

$$\begin{aligned}\mathrm{D}_\delta I(\{\boldsymbol{y}^\epsilon\};\{\boldsymbol{X}^\epsilon\}) &= \frac{1}{2}\sum_{\alpha\in\mathcal{I}_C}\sum_{\beta\in\mathcal{I}_{\mathcal{N}^\alpha}} [\partial_{\lambda^{\alpha\beta}} W_0^{\alpha\beta}\boldsymbol{e}^{\alpha\beta}]\cdot\mathrm{D}_\delta\boldsymbol{\upsilon}^{\alpha\beta} \\ &=: \frac{1}{2}\sum_{\alpha\in\mathcal{I}_C}\sum_{\beta\in\mathcal{I}_{\mathcal{N}^\alpha}} \boldsymbol{p}^{\alpha\beta}\cdot\mathrm{D}_\delta\boldsymbol{\upsilon}^{\alpha\beta} = -\sum_{\alpha\in\mathcal{I}_C}\sum_{\beta\in\mathcal{I}_{\mathcal{N}^\alpha}} \boldsymbol{p}^{\alpha\beta}\cdot\mathrm{D}_\delta\boldsymbol{y}^\alpha \doteq 0\,,\end{aligned} \tag{16}$$

and result in the atom-wise force balance (deformational equilibrium) as the corresponding Euler–Lagrange equation

$$-\sum_{\beta\in\mathcal{I}_{\mathcal{N}^\alpha}} \boldsymbol{p}^{\alpha\beta} = \boldsymbol{0} \qquad \forall\alpha\in\mathcal{I}_C \qquad \text{with} \qquad \boldsymbol{p}^{\alpha\beta} := \partial_{\lambda^{\alpha\beta}} W_0^{\alpha\beta}\,\boldsymbol{e}^{\alpha\beta}\,. \tag{17}$$

Here $\boldsymbol{p}^{\alpha\beta}$ denotes the spatial bond-wise (Piola-type) interaction force. The expression for $\boldsymbol{p}^{\alpha\beta}$ follows from the application of the chain rule and the expression $\mathrm{D}_\delta\lambda^{\alpha\beta} = \frac{1}{\Xi^{\alpha\beta}}\mathrm{D}_\delta\upsilon^{\alpha\beta} = \frac{1}{\Xi^{\alpha\beta}}\boldsymbol{e}^{\alpha\beta}\cdot\mathrm{D}_\delta\boldsymbol{\upsilon}^{\alpha\beta}$. Note the similarity of its (signed) magnitude $\partial_{\lambda^{\alpha\beta}} W_0^{\alpha\beta}$ with the definition of the Piola stress $\boldsymbol{P} = \partial_{\boldsymbol{F}} U_0$ in Eq. (5).

If the potential energy functional $I(\{\boldsymbol{Y}^\epsilon\};\{\boldsymbol{x}^\epsilon\})$ is alternatively parameterised in $\{\boldsymbol{x}^\epsilon\}$, as in Eq. $(14)_b$, its material variations d_δ can be considered, resulting in a release of potential energy $\mathcal{R} \le 0$, that is

$$\begin{aligned}\mathrm{d}_\delta I(\{\boldsymbol{Y}^\epsilon\};\{\boldsymbol{x}^\epsilon\}) &= \frac{1}{2}\sum_{\alpha\in\mathcal{I}_C}\sum_{\beta\in\mathcal{I}_{\mathcal{N}^\alpha}} [\partial_{\Lambda^{\alpha\beta}} W_t^{\alpha\beta}\boldsymbol{E}^{\alpha\beta}]\cdot\mathrm{d}_\delta\boldsymbol{Y}^{\alpha\beta} \\ &=: \frac{1}{2}\sum_{\alpha\in\mathcal{I}_C}\sum_{\beta\in\mathcal{I}_{\mathcal{N}^\alpha}} \boldsymbol{S}^{\alpha\beta}\cdot\mathrm{d}_\delta\boldsymbol{Y}^{\alpha\beta} = -\sum_{\alpha\in\mathcal{I}_C}\sum_{\beta\in\mathcal{I}_{\mathcal{N}^\alpha}} \boldsymbol{S}^{\alpha\beta}\cdot\mathrm{d}_\delta\boldsymbol{Y}^{\alpha} \\ &=: \sum_{\alpha\in\mathcal{I}_C} \boldsymbol{B}^\alpha\cdot\mathrm{d}_\delta\boldsymbol{Y}^\alpha =: \mathcal{R} \le 0\,.\end{aligned} \tag{18}$$

Here, $\boldsymbol{S}^{\alpha\beta}$ and $\boldsymbol{B}^\alpha$, respectively, denote bond- and point-wise Eshelby-type interaction forces that are power conjugated to configurational changes of the material positions $\{\boldsymbol{Y}^\epsilon\}$ of the atoms, that is

$$-\sum_{\beta\in\mathcal{I}_{\mathcal{N}^\alpha}} \boldsymbol{S}^{\alpha\beta} =: \boldsymbol{B}^\alpha \qquad \forall\alpha\in\mathcal{I}_C \qquad \text{with} \qquad \boldsymbol{S}^{\alpha\beta} := \partial_{\Lambda^{\alpha\beta}} W_t^{\alpha\beta}\,\boldsymbol{E}^{\alpha\beta}\,. \tag{19}$$

Finally, by applying the chain rule, it is illuminating to note that the (signed) magnitude of the Eshelby-type interaction force $\boldsymbol{S}^{\alpha\beta}$ can also be expressed in energy–momentum format as

$$\boldsymbol{S}^{\alpha\beta} = [W_0^{\alpha\beta} - \lambda^{\alpha\beta}\partial_{\lambda^{\alpha\beta}} W_0^{\alpha\beta}]\boldsymbol{E}^{\alpha\beta} = [W_0^{\alpha\beta} - \lambda^{\alpha\beta}p^{\alpha\beta}]\boldsymbol{E}^{\alpha\beta}\,. \tag{20}$$

The energy–momentum format of $\boldsymbol{S}^{\alpha\beta}$ mimics the structure of the energy–momentum format of the Eshelby stress $\boldsymbol{\Sigma}$ in hyperelastic continuum mechanics, see Eq. (9).

3. Peridynamics

Attention is now turned to PD and in particular to bond-based PD. To pave the way for configurational PD and the transformations between the spatial and material settings, kinematic quantities for the spatial and material motion problem are first introduced. This is followed by a presentation of the energy expressed in the different configurations and the various variations thereof.

3.1. Kinematics

In the following the spatial and material motion problems are outlined. An overview of non-local point-wise transformations which allow one to relate the point-wise (localised) force balances derived in the subsequent section in the different settings (see Fig. 7) is then presented.

3.1.1. Spatial and material bond vectors, bond length and bond stretches

PD is a non-local continuum formulation where each physical point in the material configuration $\mathcal{B}_0$ interacts with neighbouring points within a surrounding finite horizon $\mathcal{H}_0$ of radius δ_0 - see Fig. 5. The placement of a physical point in the material configuration is given by $\boldsymbol{X}$. The spatial motion of $\boldsymbol{X}$ to its position $\boldsymbol{x}$ in the spatial configuration $\mathcal{B}_t$ is given by the nonlinear map $\boldsymbol{x} = \boldsymbol{y}(\boldsymbol{X})$. The measure of the horizon δ_0 is generally the radius of a spherical neighbourhood centred at $\boldsymbol{X}$. A neighbouring physical point with position $\boldsymbol{x}^|$ in the spatial configuration is mapped from the material configuration $\boldsymbol{X}^|$ by the same map, i.e., $\boldsymbol{x}^| = \boldsymbol{y}(\boldsymbol{X}^|)$. The relative material placement is denoted by $\boldsymbol{\Xi}^| := \boldsymbol{X}^| - \boldsymbol{X}$ and the relative spatial deformation map by $\boldsymbol{\upsilon}^| := \boldsymbol{y}^| - \boldsymbol{y}$. These vectors can be written in terms of their magnitudes and unit direction vectors as

$$\boldsymbol{\Xi}^| := |\boldsymbol{X}^| - \boldsymbol{X}|\,\boldsymbol{E}^| = \Xi^|\boldsymbol{E}^| \qquad \text{and} \qquad \boldsymbol{\upsilon}^| := |\boldsymbol{y}^| - \boldsymbol{y}|\,\boldsymbol{e}^| = \upsilon^|\boldsymbol{e}^|\,. \tag{21}$$

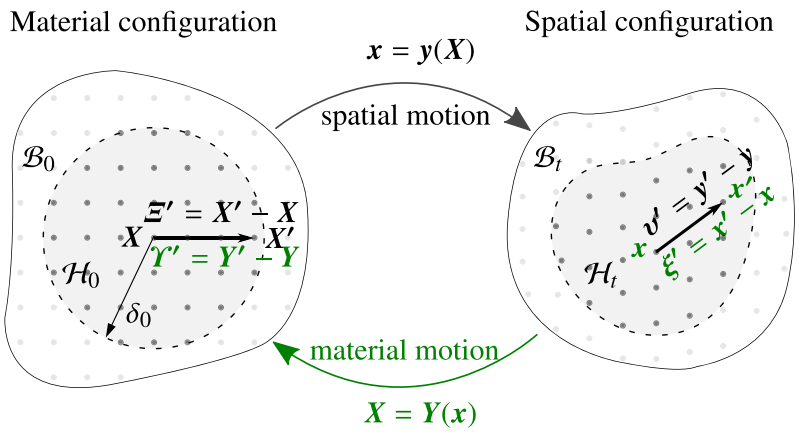

Fig. 5. Spatial and material motion of a continuum body in the peridynamic framework.

The bond stretch captures the neighbour-wise deformation and is denoted by

$$\lambda^{|} := \upsilon^{|} / \Xi^{|} . \tag{22}$$

The material motion of $\boldsymbol{x}$ to $\boldsymbol{X}$ and its neighbours from $\boldsymbol{x}^{|}$ to $\boldsymbol{X}^{|}$ can similarly be expressed using the inverse non-linear deformation map as $\boldsymbol{X} = \boldsymbol{Y}(\boldsymbol{x})$ and $\boldsymbol{X}^{|} = \boldsymbol{Y}(\boldsymbol{x}^{|})$. The relative spatial placement and the relative material deformation map associated with a material motion are denoted by $\boldsymbol{\xi}^{|} := \boldsymbol{x}^{|} - \boldsymbol{x}$ and $\boldsymbol{Y}^{|} := \boldsymbol{Y}^{|} - \boldsymbol{Y}$, respectively. Again, these vectors can be written in terms of their magnitudes and unit direction vectors as

$$\boldsymbol{\xi}^{|} := |\boldsymbol{x}^{|} - \boldsymbol{x}|\, \boldsymbol{e}^{|} = \xi^{|} \boldsymbol{e}^{|} \qquad \text{and} \qquad \boldsymbol{Y}^{|} := |\boldsymbol{Y}^{|} - \boldsymbol{Y}|\, \boldsymbol{E}^{|} = Y^{|} \boldsymbol{E}^{|} . \tag{23}$$

The bond stretch from this perspective is then denoted by

$$\Lambda^{|} := Y^{|} / \xi^{|} . \tag{24}$$

Remark 2. Note the concepts borrowed from molecular mechanics present in the (non-local) continuum formulation of PD. Clearly, the atomistic cut-off radius translates into the PD horizon radius δ_0, the concept of atomistic bonds of finite cardinality translates into a continuous distribution of PD bonds within the horizon $\mathcal{H}_0$, and summation over the atomistic cardinality of bonds translates into integration over the PD horizon $\mathcal{H}_0$. □

Remark 3. In PD quantities can be expressed as neighbour-wise, point-wise and total measures. Each physical point interacts with all neighbouring points within its horizon. Measures calculated between a point and one of its neighbours are called neighbour-wise quantities. The integral of these neighbour-wise quantities over the horizon results in point-wise quantities (non-local measures). Finally integrating a point-wise quantity over the entire domain occupied by a body results in the total quantity for the body. □

Remark 4. The conventional deformation gradient $\boldsymbol{F}$ from classical continuum mechanics (CCM) in Eq. $(1)_a$ is a spatial *tangent* map that can be viewed as a linear transformation of an *infinitesimal* line element $\mathrm{d}\boldsymbol{X}$ from the material (tangent) configuration to its counterparts $\mathrm{d}\boldsymbol{x}$ in the spatial configuration. In the PD framework, a linear transformation of a *finite* line element $\boldsymbol{\Xi}^{|}$ from the material configuration to its counterpart in the spatial configuration $\boldsymbol{\upsilon}^{|}$ is given by the neighbour-wise spatial *secant* map, that is

$$\boldsymbol{\upsilon}^{|} = \mathbb{F}^{|} \cdot \boldsymbol{\Xi}^{|} \qquad \text{with} \qquad \mathbb{F}^{|} := \lambda^{|} \boldsymbol{e}^{|} \otimes \boldsymbol{E}^{|} . \tag{25}$$

Likewise a finite line element in the spatial configuration $\boldsymbol{\xi}^{|}$ can be mapped to its counterpart in the material configuration $\boldsymbol{Y}^{|}$ via the neighbour-wise material secant map, that is

$$\boldsymbol{Y}^{|} = \mathbb{f}^{|} \cdot \boldsymbol{\xi}^{|} \qquad \text{with} \qquad \mathbb{f}^{|} := \Lambda^{|} \boldsymbol{E}^{|} \otimes \boldsymbol{e}^{|} . \tag{26}$$

These relations are useful in subsequent neighbour-wise expressions but cannot be simply extended by integrating over the horizon to produce meaningful point-wise quantities. □

3.1.2. The concept of bond number double-density

The potential energy contribution of a point (atom) in a discrete atomistic system is calculated by a *summation* over the neighbouring bonds (see Eq. (14)). The extension of this format to PD provides the motivation for the concept of *bond number double-density*. The material and spatial bond number *double-densities*, $\varrho_0^{|}$ and $\varrho_t^{|}$, respectively, denote the density of bonds per volume in the horizon *and* per volume of the body, in the material and the spatial configuration, respectively. Their units are $[\varrho_0^{|}] = [\varrho_t^{|}] = \text{bonds/m}^6$. As a consequence, integrating the bond number double-densities over the volume of the horizon is equivalent to integrating over the *bond number densities* $N^{|}$ and $n^{|}$ with corresponding differential elements $\mathrm{d}N^{|} = \varrho_0^{|} \mathrm{d}V^{|}$ and $\mathrm{d}n^{|} = \varrho_t^{|} \mathrm{d}\upsilon^{|}$, respectively. That is,

$$\int_{\mathcal{N}_0} \mathrm{d}N^{|} = \int_{\mathcal{H}_0} \varrho_0^{|} \mathrm{d}V^{|} \qquad \text{and} \qquad \int_{\mathcal{N}_t} \mathrm{d}n^{|} = \int_{\mathcal{H}_t} \varrho_t^{|} \mathrm{d}\upsilon^{|} . \tag{27}$$

Note that $N^{|}$ and $n^{|}$ are point-wise bond number densities of units $[N^{|}] = [n^{|}] = \text{bonds/m}^3$, thus integrating them over the entire body yields the total number of bonds - a finite, countable number. Using the volume ratios for infinitesimal point-wise volumes from $(1)_{c-d}$, the point-wise bond number densities $N^{|}$ and $n^{|}$ are related as

$$J \int_{\mathcal{N}_t} \mathrm{d}n^{|} = \int_{\mathcal{N}_0} \mathrm{d}N^{|} \qquad \text{and} \qquad \int_{\mathcal{N}_t} \mathrm{d}n^{|} = j \int_{\mathcal{N}_0} \mathrm{d}N^{|} . \tag{28}$$

Clearly, this relation is analogous to the relation between point-wise densities in CCM. For the sake of simplicity, but without loss of generality, the material bond number double-density $\varrho_0^{|}$ is taken as a constant within the horizon $\mathcal{H}_0$ in the sequel.

3.1.3. Gradients of the relative spatial and material deformation maps within the horizon

This section details the derivation of the *relative* gradients of the relative spatial and material deformation maps $\boldsymbol{\upsilon}^{|}$ and $\boldsymbol{Y}^{|}$, respectively, i.e., the gradients of $\boldsymbol{\upsilon}^{|}$ and $\boldsymbol{Y}^{|}$ with respect to the relative material and spatial placements $\boldsymbol{\Xi}^{|}$ and $\boldsymbol{\xi}^{|}$, respectively, in the horizon. To abbreviate terminology, these shall also be denoted as the *horizon gradients*. The horizon gradients constitute crucial expressions in the formulation of the pull-back and push-forward operations between the spatial and material settings of the point-wise force balances derived in Section 3.3. The relative material gradient of the relative spatial deformation, in

short the *horizon deformation gradient*, is for example analogous to the local deformation gradient in Eq. $(1)_a$, however in the geometry of the horizon of a point.

The relative spatial deformation map $\boldsymbol{\upsilon}^{|} = \boldsymbol{y}^{|} - \boldsymbol{y}$ (the bond vector pointing from a point to its neighbour in the spatial configuration) for a smooth deformation in $\mathcal{H}_0$ can be expressed via a Taylor series expansion by

$$\begin{aligned}\boldsymbol{\upsilon}^{|} &= \frac{1}{1!}\frac{\partial \boldsymbol{y}}{\partial \boldsymbol{X}}\Big|_{\boldsymbol{X}} \cdot \boldsymbol{\Xi}^{|} + \frac{1}{2!}\frac{\partial^2 \boldsymbol{y}}{\partial \boldsymbol{X}\otimes\partial \boldsymbol{X}}\Big|_{\boldsymbol{X}} : \left[\boldsymbol{\Xi}^{|}\otimes\boldsymbol{\Xi}^{|}\right] \\ &\quad + \frac{1}{3!}\frac{\partial^3 \boldsymbol{y}}{\partial \boldsymbol{X}\otimes\partial \boldsymbol{X}\otimes\partial \boldsymbol{X}}\Big|_{\boldsymbol{X}} \cdot : \left[\boldsymbol{\Xi}^{|}\otimes\boldsymbol{\Xi}^{|}\otimes\boldsymbol{\Xi}^{|}\right] + \cdots \\ &= \frac{1}{1!}\boldsymbol{F}\cdot\boldsymbol{\Xi}^{|} + \frac{1}{2!}\nabla_{\boldsymbol{X}}\boldsymbol{F} : \left[\boldsymbol{\Xi}^{|}\otimes\boldsymbol{\Xi}^{|}\right] \\ &\quad + \frac{1}{3!}\nabla^2_{\boldsymbol{X}}\boldsymbol{F}\cdot : \left[\boldsymbol{\Xi}^{|}\otimes\boldsymbol{\Xi}^{|}\otimes\boldsymbol{\Xi}^{|}\right] + \cdots .\end{aligned} \tag{29}$$

In the second step above, the Taylor series is written in terms of the classical deformation gradient and its higher order gradients. The *material horizon gradient*, i.e., the relative material gradient $\nabla_{\boldsymbol{\Xi}^{|}}$ of the relative spatial deformation $\boldsymbol{\upsilon}^{|}$, yields the *horizon deformation gradient* $\boldsymbol{\Phi}^{|}$ as follows

$$\begin{aligned}\boldsymbol{\Phi}^{|} = \frac{\partial \boldsymbol{\upsilon}^{|}}{\partial \boldsymbol{\Xi}^{|}} &= \frac{1}{0!}\frac{\partial \boldsymbol{y}}{\partial \boldsymbol{X}}\Big|_{\boldsymbol{X}} + \frac{1}{1!}\frac{\partial^2 \boldsymbol{y}}{\partial \boldsymbol{X}\otimes\partial \boldsymbol{X}}\Big|_{\boldsymbol{X}} \cdot\boldsymbol{\Xi}^{|} \\ &\quad + \frac{1}{2!}\frac{\partial^3 \boldsymbol{y}}{\partial \boldsymbol{X}\otimes\boldsymbol{X}\otimes\boldsymbol{X}}\Big|_{\boldsymbol{X}} : \left[\boldsymbol{\Xi}^{|}\otimes\boldsymbol{\Xi}^{|}\right] + \cdots \\ &= \frac{1}{0!}\boldsymbol{F} + \frac{1}{1!}\nabla_{\boldsymbol{X}}\boldsymbol{F}\cdot\boldsymbol{\Xi}^{|} + \frac{1}{2!}\nabla^2_{\boldsymbol{X}}\boldsymbol{F} : \left[\boldsymbol{\Xi}^{|}\otimes\boldsymbol{\Xi}^{|}\right] + \cdots \\ &=: \boldsymbol{F} + \boldsymbol{F}^{\odot} .\end{aligned} \tag{30}$$

The horizon deformation gradient decomposes into the local deformation gradient $\boldsymbol{F}$ from $(1)_a$ and a contribution $\boldsymbol{F}^{\odot}$ capturing non-locality due to the finite size of the horizon. Note that for the case where $\delta_0 \to 0$, i.e., the neighbourhood shrinks to zero, the local deformation gradient in $(1)_a$ is recovered as $\boldsymbol{\Phi}^{|}|_{\delta_0\to 0} = \boldsymbol{F}$ with $\boldsymbol{F}^{\odot}|_{\delta_0\to 0} = \boldsymbol{0}$.

Similarly, the relative material deformation map $\boldsymbol{\Upsilon}^{|} = \boldsymbol{Y}^{|} - \boldsymbol{Y}$ for a smooth deformation in $\mathcal{H}_t$ can be expressed in a Taylor series expansion as

$$\begin{aligned}\boldsymbol{\Upsilon}^{|} &= \frac{1}{1!}\frac{\partial \boldsymbol{Y}}{\partial \boldsymbol{x}}\Big|_{\boldsymbol{x}} \cdot\boldsymbol{\xi}^{|} + \frac{1}{2!}\frac{\partial^2 \boldsymbol{Y}}{\partial \boldsymbol{x}\otimes\partial \boldsymbol{x}}\Big|_{\boldsymbol{x}} : \left[\boldsymbol{\xi}^{|}\otimes\boldsymbol{\xi}^{|}\right] \\ &\quad + \frac{1}{3!}\frac{\partial^3 \boldsymbol{Y}}{\partial \boldsymbol{x}\otimes\partial \boldsymbol{x}\otimes\partial \boldsymbol{x}}\Big|_{\boldsymbol{x}} \cdot : \left[\boldsymbol{\xi}^{|}\otimes\boldsymbol{\xi}^{|}\otimes\boldsymbol{\xi}^{|}\right] + \cdots \\ &= \frac{1}{1!}\boldsymbol{f}\cdot\boldsymbol{\xi}^{|} + \frac{1}{2!}\nabla_{\boldsymbol{x}}\boldsymbol{f} : \left[\boldsymbol{\xi}^{|}\otimes\boldsymbol{\xi}^{|}\right] + \frac{1}{3!}\nabla^2_{\boldsymbol{x}}\boldsymbol{f}\cdot : \left[\boldsymbol{\xi}^{|}\otimes\boldsymbol{\xi}^{|}\otimes\boldsymbol{\xi}^{|}\right] + \cdots .\end{aligned} \tag{31}$$

The *spatial horizon gradient*, i.e., the relative spatial gradient $\nabla_{\boldsymbol{\xi}^{|}}$ of $\boldsymbol{\Upsilon}^{|}$, results in the *horizon deformation gradient* $\boldsymbol{\phi}^{|}$, given by

$$\begin{aligned}\boldsymbol{\phi}^{|} = \frac{\partial \boldsymbol{\Upsilon}^{|}}{\partial \boldsymbol{\xi}^{|}} &= \frac{1}{0!}\frac{\partial \boldsymbol{Y}}{\partial \boldsymbol{x}}\Big|_{\boldsymbol{x}} + \frac{1}{1!}\frac{\partial^2 \boldsymbol{Y}}{\partial \boldsymbol{x}\otimes\partial \boldsymbol{x}}\Big|_{\boldsymbol{x}} \cdot\boldsymbol{\xi}^{|} \\ &\quad + \frac{1}{2!}\frac{\partial^3 \boldsymbol{Y}}{\partial \boldsymbol{x}\otimes\partial \boldsymbol{x}\otimes\partial \boldsymbol{x}}\Big|_{\boldsymbol{x}} : \left[\boldsymbol{\xi}^{|}\otimes\boldsymbol{\xi}^{|}\right] + \cdots \\ &= \frac{1}{0!}\boldsymbol{f} + \frac{1}{1!}\nabla_{\boldsymbol{x}}\boldsymbol{f}\cdot\boldsymbol{\xi}^{|} + \frac{1}{2!}\nabla^2_{\boldsymbol{x}}\boldsymbol{f} : \left[\boldsymbol{\xi}^{|}\otimes\boldsymbol{\xi}^{|}\right] + \cdots \\ &=: \boldsymbol{f} + \boldsymbol{f}^{\odot} .\end{aligned} \tag{32}$$

Note that for the case of vanishing horizon size $\delta_t \to 0$ the inverse deformation gradient given in Eq. $(1)_b$ is recovered as $\boldsymbol{\phi}^{|}|_{\delta_t\to 0} = \boldsymbol{f}$ with $\boldsymbol{f}^{\odot}|_{\delta_t\to 0} = \boldsymbol{0}$.

3.2. Potential energy functional and its spatial and material variations

The potential energy of a body, and specifically the variation of this energy, is the base from which both the spatial and material point-wise force balances and subsequently the energy release upon configurational changes can be explored. This section outlines various ways of expressing the potential energy functional, the different variations of these expressions and defines the resulting energy conjugate quantities. Finally, by exploiting the *property* that the potential energy density on the boundary of the horizon vanishes, some inferences relevant to transforming spatial and material point-wise force balances are made.

3.2.1. Potential energy functional

In PD, the potential energy functional I of a body can be expressed, just like in CCM, in two versions by interchanging the role of field and parameterisation, i.e., $I = I(\boldsymbol{y};\boldsymbol{X})$ or $I = I(\boldsymbol{Y};\boldsymbol{x})$. For the sake of presentation contributions to the external potential energy are neglected in the sequel (i.e., external spatial forces are zero). In contrast to CCM where the point-wise potential energy density per volume is a local quantity, the point-wise potential energy density in PD is a non-local quantity, i.e., it is expressed in terms of the integral of a potential energy double-density over the horizon. In the sequel, the potential energy double-density is expressed via the neighbour-wise bond energy densities $w_0^{|}$ and $w_t^{|}$ per lengths $\Xi^{|}$ and $\xi^{|}$ in the material and spatial configurations, respectively. Thus the bond energy densities are related by the bond stretches in Eqs. (22) and (24), i.e., $w_0^{|} = w_t^{|}\lambda^{|}$ and $w_t^{|} = w_0^{|}\Lambda^{|}$. For the sake of simplicity, and to emphasise the contribution of the non-local material body force which emerges as the defining quantity for energy release in Section 3.2.2, the dependence of the bond energy densities is furthermore restricted to $w_0^{|} = w_0^{|}(\lambda^{|})$ and $w_t^{|} = w_t^{|}(\Lambda^{|})$. Thus, specifically, $w_0^{|} \neq w_0^{|}(\boldsymbol{X})$ and $w_t^{|} \neq w_t^{|}(\boldsymbol{Y})$. As a consequence, material body forces accounting for material inhomogeneities, analogous to Eqs. (7)–(8) in CCM, are neglected. Taken together, the potential energy functional reads eventually as

$$\begin{aligned}I(\boldsymbol{y};\boldsymbol{X}) &= \frac{1}{2}\int_{\mathcal{B}_0}\int_{\mathcal{N}_0} w_0^{|}(\lambda^{|})\Xi^{|}\,\mathrm{d}N^{|}\,\mathrm{d}V , \\ I(\boldsymbol{Y};\boldsymbol{x}) &= \frac{1}{2}\int_{\mathcal{B}_t}\int_{\mathcal{N}_t} w_t^{|}(\Lambda^{|})\xi^{|}\,\mathrm{d}n^{|}\,\mathrm{d}v .\end{aligned} \tag{33}$$

These representations should be compared to the corresponding expressions for the potential energy functional for the discrete atomistic case in Eq. (14). Observe that by using Eq. (28), the point-wise potential energy densities in the material and spatial configuration are related by

$$\begin{aligned}J\int_{\mathcal{N}_t} w_t^{|}\,\xi^{|}\,\mathrm{d}n^{|} &= \int_{\mathcal{N}_0} w_0^{|}\,\Xi^{|}\,\mathrm{d}N^{|} , \\ j\int_{\mathcal{N}_0} w_0^{|}\,\Xi^{|}\,\mathrm{d}N^{|} &= \int_{\mathcal{N}_t} w_t^{|}\,\xi^{|}\,\mathrm{d}n^{|} .\end{aligned} \tag{34}$$

Remark 5. With the aid of the material and spatial bond number double-densities $\varrho_0^{|}$ and $\varrho_t^{|}$ in Eq. (27), the point-wise non-local potential energy density expressed as integrals over either $\mathcal{N}_0$ and $\mathcal{N}_t$ in Eq. (33) can alternatively be written, in a perhaps more familiar form, as integrals over the horizon $\mathcal{H}_0$ or $\mathcal{H}_t$ as

$$\begin{aligned}I(\boldsymbol{y};\boldsymbol{X}) &= \frac{1}{2}\int_{\mathcal{B}_0}\int_{\mathcal{H}_0} w_0^{|}(\lambda^{|})\Xi^{|}\varrho_0^{|}\,\mathrm{d}V^{|}\,\mathrm{d}V , \\ I(\boldsymbol{Y};\boldsymbol{x}) &= \frac{1}{2}\int_{\mathcal{B}_t}\int_{\mathcal{H}_t} w_t^{|}(\Lambda^{|})\xi^{|}\varrho_t^{|}\,\mathrm{d}v^{|}\,\mathrm{d}v .\end{aligned} \tag{35}$$

Note that $w_0^{|}\Xi^{|}\varrho_0^{|}$ and $w_t^{|}\Xi\varrho_t^{|}$ are potential energy double-densities, i.e., densities per volume in the horizon and per volume in the body. In the sequel this interchange of integrals over $\mathcal{N}_0$ and $\mathcal{N}_t$ and integrals over $\mathcal{H}_0$ and $\mathcal{H}_t$ by involving the bond number double-densities is performed routinely and without further mention. □

3.2.2. Spatial and material variations of the potential energy functional

In analogy to the process outlined in the preceding sections, a spatial variation of the potential energy functional $I(\boldsymbol{y};\boldsymbol{X})$ in Eq. $(33)_a$ renders the stationary point $\mathrm{D}_\delta I(\boldsymbol{y};\boldsymbol{X}) \doteq 0$ as

$$\begin{aligned}\mathrm{D}_\delta I(\boldsymbol{y};\boldsymbol{X}) &= \frac{1}{2}\int_{\mathcal{B}_0}\int_{\mathcal{N}_0} \partial_{\lambda^{|}} w_0^{|}\,\boldsymbol{e}^{|}\cdot\mathrm{D}_\delta\boldsymbol{\upsilon}^{|}\,\mathrm{d}N^{|}\,\mathrm{d}V \\ &=: \frac{1}{2}\int_{\mathcal{B}_0}\int_{\mathcal{N}_0} \boldsymbol{p}^{|}\cdot\mathrm{D}_\delta\boldsymbol{\upsilon}^{|}\,\mathrm{d}N^{|}\,\mathrm{d}V \\ &= -\int_{\mathcal{B}_0}\int_{\mathcal{N}_0} \boldsymbol{p}^{|}\,\mathrm{d}N^{|}\cdot\mathrm{D}_\delta\boldsymbol{y}\,\mathrm{d}V \doteq 0 ,\end{aligned} \tag{36}$$

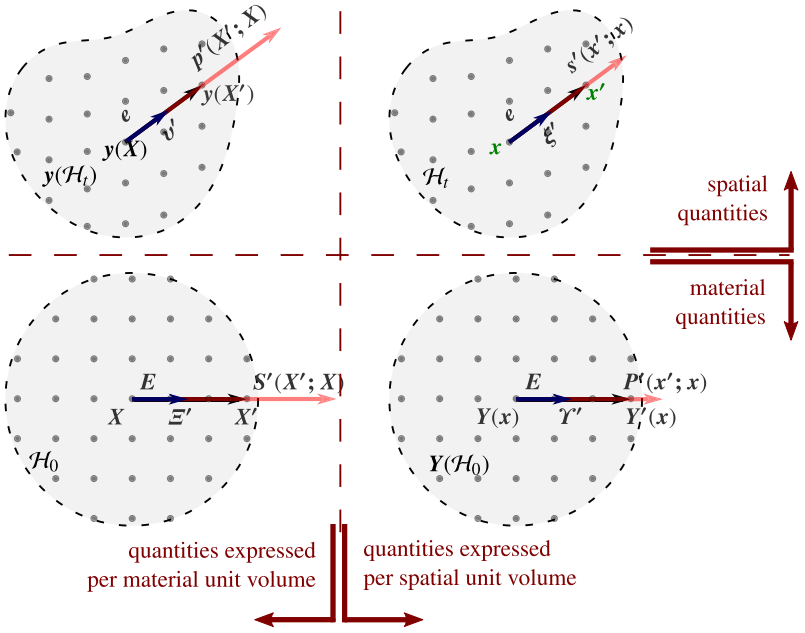

Fig. 6. Material and spatial bond-wise interaction forces depicted in their associated configurations and parameterisations.

and yields the point-wise force balance (deformational equilibrium) as the corresponding Euler–Lagrange equations:

$$-\int_{\mathcal{N}_0} \boldsymbol{p}^{\shortmid}\,\mathrm{d}N^{\shortmid} = \boldsymbol{0} \qquad \text{with} \qquad \boldsymbol{p}^{\shortmid} := \partial_{\lambda^{\shortmid}} w_0^{\shortmid}\,\boldsymbol{e}^{\shortmid}\,. \tag{37}$$

Here $\boldsymbol{p}^{\shortmid}$ denotes the spatial bond-wise (Piola-type) interaction force of unit $[\boldsymbol{p}^{\shortmid}]$ = force/bond with integral over $\mathcal{N}_0$ rendering a point-wise force density of unit force/m^3. Note the similarity of its (signed) magnitude $\partial_{\lambda^{\shortmid}} w_0^{\shortmid}$ with the definition of the Piola stress $\boldsymbol{P} = \partial_{\boldsymbol{F}} U_0$ in Eq. (5) and the definition of the atomistic spatial bond-wise (Piola-type) interaction force $p^{\alpha\beta} = \partial_{\lambda^{\alpha\beta}} W_0^{\alpha\beta}$ in Eq. (17). The expression for $\boldsymbol{p}^{\shortmid}$ follows from application of the chain rule and the expression $\mathrm{D}_\delta \lambda^{\shortmid} = \frac{1}{\Xi^{\shortmid}} \mathrm{D}_\delta \upsilon^{\shortmid} = \frac{1}{\Xi^{\shortmid}} \boldsymbol{e}^{\shortmid} \cdot \mathrm{D}_\delta \boldsymbol{\upsilon}^{\shortmid}$.

Remark 6. The last step in Eq. (36) is motivated by the same procedure as employed in discrete atomistic systems and thus follows a slightly different rationale as put forward in Javili et al. (2019a). The key steps are as follows: (i) express the integral over $\mathcal{N}_0$ by an integral over $\mathcal{H}_0$ by using $\mathrm{d}N^{\shortmid} = \varrho_0^{\shortmid}\mathrm{d}V^{\shortmid}$, ii) extend the resulting integral over $\mathcal{H}_0$ to an integral over the entire body $\mathcal{B}_0$ due to the definition of the horizon, iii) expand the spatial variation of the spatial bond vector $\mathrm{D}_\delta \boldsymbol{\upsilon}^{\shortmid} = \mathrm{D}_\delta \boldsymbol{y}^{\shortmid} - \mathrm{D}_\delta \boldsymbol{y}$ thereby resulting in two terms, iv) exchange the labelling of $\mathrm{d}V$ and $\mathrm{d}V^{\shortmid}$ in the first term and consider *actio est reactio* for the bond-wise interaction forces $\boldsymbol{p} = -\boldsymbol{p}^{\shortmid}$, and (v) exchange the sequence of integrals in the first term to finally assemble the result. □

Note that the bond-wise interaction force $\boldsymbol{p}^{\shortmid} = \boldsymbol{p}^{\shortmid}(\boldsymbol{X}^{\shortmid}; \boldsymbol{X})$ is a spatial quantity with material parameterisation, i.e., it is parameterised by material placements $\boldsymbol{X}^{\shortmid}$ and $\boldsymbol{X}$ as depicted in Fig. 6. Thus when taking the integral over $\mathcal{N}_0$, all bonds (expressed in terms of their point-wise density per material unit volume) within the horizon are visited as parameterised by their material placements. One can thus re-parameterise the bond-wise interaction force $\boldsymbol{p}^{\shortmid} = \boldsymbol{p}^{\shortmid}(\boldsymbol{X}^{\shortmid}; \boldsymbol{X})$ in terms of spatial placements $\boldsymbol{x}^{\shortmid}$ and $\boldsymbol{x}$ as $\boldsymbol{s}^{\shortmid} = \boldsymbol{s}^{\shortmid}(\boldsymbol{x}^{\shortmid}; \boldsymbol{x}) := \boldsymbol{p}^{\shortmid} \circ \boldsymbol{Y}(\boldsymbol{x})$, see Fig. 6. As a consequence, the spatial variation of the potential energy functional can be written equivalently in terms of the spatial bond-wise Cauchy-type interaction force $\boldsymbol{s}^{\shortmid} = \boldsymbol{s}^{\shortmid}(\boldsymbol{x}^{\shortmid}; \boldsymbol{x})$ (that is here introduced to PD for the first time) as

$$\begin{aligned} -\int_{\mathcal{B}_0}\int_{\mathcal{N}_0} \boldsymbol{p}^{\shortmid}\,\mathrm{d}N^{\shortmid} \cdot \mathrm{D}_\delta \boldsymbol{y}\,\mathrm{d}V &= -\int_{\mathcal{B}_t}\int_{\mathcal{N}_t} \boldsymbol{s}^{\shortmid}\,\mathrm{d}n^{\shortmid} \cdot \mathrm{D}_\delta \boldsymbol{y}\,\mathrm{d}v \\ \text{thus} \qquad -\int_{\mathcal{N}_t} \boldsymbol{s}^{\shortmid}\,\mathrm{d}n^{\shortmid} &= \boldsymbol{0}\,. \end{aligned} \tag{38}$$

Using the volume map from CCM $(1)_d$ and noticing that the inner integrals in the above are essentially the same point-wise force density expressed either per material unit volume in $\mathcal{B}_0$ or per spatial unit volume in $\mathcal{B}_t$, a Piola-type transformation of the resulting point-wise force density can be identified as

$$j\int_{\mathcal{N}_0} \boldsymbol{p}^{\shortmid}\,\mathrm{d}N^{\shortmid} = \int_{\mathcal{N}_t} \boldsymbol{s}^{\shortmid}\,\mathrm{d}n^{\shortmid} \qquad \text{with} \qquad \boldsymbol{s}^{\shortmid} := \boldsymbol{p}^{\shortmid} \circ \boldsymbol{Y}(\boldsymbol{x})\,. \tag{39}$$

Note that different to the Piola transform for second-order tensors that involves the cofactor of the deformation gradient, for the point-wise vectorial force densities only the Jacobian is involved.

If the potential energy functional $I(\boldsymbol{Y}; \boldsymbol{x})$ is alternatively parameterised in $\boldsymbol{x}$ as in Eq. $(35)_b$ its material variation d_δ can be considered, resulting in a release of potential energy $\mathcal{R} \leq 0$, that is

$$\begin{aligned} \mathrm{d}_\delta I(\boldsymbol{Y}; \boldsymbol{x}) &= \frac{1}{2}\int_{\mathcal{B}_t}\int_{\mathcal{N}_t} \partial_{\Lambda^{\shortmid}} w_t^{\shortmid}\,\boldsymbol{E}^{\shortmid} \cdot \mathrm{d}_\delta \boldsymbol{Y}^{\shortmid}\,\mathrm{d}n^{\shortmid}\,\mathrm{d}v \\ &=: \frac{1}{2}\int_{\mathcal{B}_t}\int_{\mathcal{N}_t} \boldsymbol{P}^{\shortmid} \cdot \mathrm{d}_\delta \boldsymbol{Y}^{\shortmid}\,\mathrm{d}n^{\shortmid}\,\mathrm{d}v = -\int_{\mathcal{B}_t}\int_{\mathcal{N}_t} \boldsymbol{P}^{\shortmid}\,\mathrm{d}n^{\shortmid} \cdot \mathrm{d}_\delta \boldsymbol{Y}\,\mathrm{d}v \\ &=: \int_{\mathcal{B}_t} \boldsymbol{B}_t^{\odot} \cdot \mathrm{d}_\delta \boldsymbol{Y}\,\mathrm{d}v =: \mathcal{R} \leq 0\,. \end{aligned} \tag{40}$$

Here, $\boldsymbol{P}^{\shortmid}$ and $\boldsymbol{B}_t^{\odot}$, respectively denote the material bond-wise Piola-type interaction force and the resulting material point-wise force density that are power conjugated to configurational changes of the material positions $\mathrm{d}_\delta \boldsymbol{Y}$ of the physical points constituting the body, that is

$$-\int_{\mathcal{N}_t} \boldsymbol{P}^{\shortmid}\,\mathrm{d}n^{\shortmid} =: \boldsymbol{B}_t^{\odot} \qquad \text{with} \qquad \boldsymbol{P}^{\shortmid} := \partial_{\Lambda^{\shortmid}} w_t^{\shortmid}\,\boldsymbol{E}^{\shortmid}\,. \tag{41}$$

An equivalent expression for the material variation of the potential energy functional with material parameterisation can be written in terms of the material bond-wise Eshelby-type interaction force $\boldsymbol{S}^{\shortmid} = \boldsymbol{S}^{\shortmid}(\boldsymbol{X}^{\shortmid}; \boldsymbol{X}) := \boldsymbol{P}^{\shortmid} \circ \boldsymbol{y}(\boldsymbol{X})$ as

$$\begin{aligned} -\int_{\mathcal{B}_t}\int_{\mathcal{N}_t} \boldsymbol{P}^{\shortmid}\,\mathrm{d}n^{\shortmid} \cdot \mathrm{d}_\delta \boldsymbol{Y}\,\mathrm{d}v &= -\int_{\mathcal{B}_0}\int_{\mathcal{N}_0} \boldsymbol{S}^{\shortmid}\,\mathrm{d}N^{\shortmid} \cdot \mathrm{d}_\delta \boldsymbol{Y}\,\mathrm{d}V \\ \text{thus} \qquad -\int_{\mathcal{N}_0} \boldsymbol{S}^{\shortmid}\,\mathrm{d}N^{\shortmid} &=: \boldsymbol{B}_0^{\odot}\,. \end{aligned} \tag{42}$$

Recalling that $\boldsymbol{B}_0^{\odot}$ and $\boldsymbol{B}_t^{\odot}$ denote the same point-wise force density expressed either per material unit volume in $\mathcal{B}_0$ or per spatial unit volume in $\mathcal{B}_t$, respectively, a Piola-type transformation of the resulting point-wise force density can finally be identified as

$$J \int_{\mathcal{N}_t} \boldsymbol{P}^{|} \, \mathrm{d}n^{|} = \int_{\mathcal{N}_0} \boldsymbol{S}^{|} \, \mathrm{d}N^{|} \qquad \text{with} \qquad \boldsymbol{S}^{|} := \boldsymbol{P}^{|} \circ \boldsymbol{y}(\boldsymbol{X}) \,. \tag{43}$$

3.2.3. Energy–momentum format of spatial and material bond-wise interaction forces

The spatial bond-wise Cauchy-type interaction force $\boldsymbol{s}^{|}$ can also be written in energy–momentum format in terms of $w_t^{|}$ using the fact that $\boldsymbol{s}^{|}$ and $\boldsymbol{p}^{|}$ are essentially the same measure parameterised in either $\boldsymbol{x}$ or $\boldsymbol{X}$, respectively, together with the product and chain rule

$$\boldsymbol{s}^{|}(\boldsymbol{x}^{|};\boldsymbol{x}) := \boldsymbol{p}^{|} \circ \boldsymbol{Y}(\boldsymbol{x}) = \left[w_t^{|} - \Lambda^{|} \partial_{\Lambda^{|}} w_t^{|} \right] \boldsymbol{e}^{|} \quad \Rightarrow \quad \boldsymbol{s}^{|} = w_t^{|} \boldsymbol{e}^{|} - \mathbb{F}^{|\mathrm{t}} \cdot \boldsymbol{P}^{|} \,. \tag{44}$$

Here the presentation in terms of $\boldsymbol{P}^{|}$ and $\mathbb{F}^{|}$ is due to Eq. $(41)_b$ and the abbreviation in Eq. (26). Note that this format for $\boldsymbol{s}^{|}$ compares favourably to the energy–momentum format of the Cauchy stress $\boldsymbol{\sigma}$ in CCM.

Likewise, the material bond-wise Eshelby-type interaction force $\boldsymbol{S}^{|}$ can also be written in energy–momentum format in terms of $w_0^{|}$ using the fact that $\boldsymbol{S}^{|}$ and $\boldsymbol{P}^{|}$ are essentially the same measure parameterised in either $\boldsymbol{X}$ or $\boldsymbol{x}$, respectively, together with the product and chain rule

$$\boldsymbol{S}^{|}(\boldsymbol{X}^{|};\boldsymbol{X}) := \boldsymbol{P}^{|} \circ \boldsymbol{y}(\boldsymbol{X}) = \left[w_0^{|} - \lambda^{|} \partial_{\lambda^{|}} w_0^{|} \right] \boldsymbol{E}^{|} \Rightarrow \boldsymbol{S}^{|} = w_0^{|} \boldsymbol{E}^{|} - \mathbb{F}^{|\mathrm{t}} \cdot \boldsymbol{p}^{|} \,. \tag{45}$$

Here the presentation in terms of $\boldsymbol{p}^{|}$ and $\mathbb{F}^{|}$ is due to Eq. $(37)_b$ and the abbreviation in Eq. (25). Note that this format for $\boldsymbol{S}^{|}$ is comparable to the energy–momentum format of the Eshelby stress $\boldsymbol{\Sigma}$ in CCM (9).

3.3. Relating spatial and material point-wise force densities

With the aim of determining a relation between spatial and material point-wise force densities, the Gauss theorem on the horizon is considered. The integral on the boundary of the horizon of an arbitrary density $u_0^{|}$ can be expressed using the Gauss theorem by

$$\int_{\partial\mathcal{H}_0} u_0^{|} \mathrm{d}\boldsymbol{A}^{|} = \int_{\mathcal{H}_0} \mathrm{Div}_{\Xi^{|}} (u_0^{|} \boldsymbol{I}) \, \mathrm{d}V^{|} = \int_{\mathcal{H}_0} \nabla_{\Xi^{|}} u_0^{|} \, \mathrm{d}V^{|} , \tag{46}$$

where $\nabla_{\Xi^{|}}$ is the gradient with respect to the relative coordinates of the horizon in the material configuration, i.e., the *material horizon gradient*.

Recall that in PD the bond-wise interactions between points are restricted to a finite neighbourhood $\mathcal{H}_0$. In other words, the contributions to the potential energy are zero from points outside $\mathcal{H}_0$, i.e., the bond energy density per length $w_0^{|}$ is zero on $\partial\mathcal{H}_0$ (the decay to zero on $\partial\mathcal{H}_0$ is assumed smooth but may otherwise be arbitrarily abrupt). With this, applying the Gauss theorem to the integral of the potential energy double-density on the boundary of the horizon renders

$$\int_{\partial\mathcal{H}_0} \left[w_0^{|} \, \Xi^{|} \, \varrho_0^{|} \right] \mathrm{d}\boldsymbol{A}^{|} = \int_{\mathcal{N}_0} \nabla_{\Xi^{|}} \left(w_0^{|} \, \Xi^{|} \right) \mathrm{d}N^{|} \equiv \boldsymbol{0} \,. \tag{47}$$

Here, the assumption that the material bond number double-density is constant within the horizon, i.e., $\varrho_0^{|} \neq \varrho_0^{|}(\boldsymbol{\Xi}^{|})$, has directly been incorporated into the second term. Recalling next that $w_0^{|} = w_0^{|}(\lambda^{|})$, i.e., $w_0^{|} \neq w_0^{|}(\boldsymbol{\Xi}^{|})$, and noting that $\nabla_{\Xi^{|}} \Xi^{|} = \boldsymbol{E}^{|}$, the material horizon gradient of the bond-wise potential energy can be calculated using the product and chain rules as

$$\nabla_{\Xi^{|}} \left(w_0^{|} \, \Xi^{|} \right) = \partial_{\lambda^{|}} w_0^{|} \, \nabla_{\Xi^{|}} \lambda^{|} \, \Xi^{|} + w_0^{|} \, \boldsymbol{E}^{|} \,. \tag{48}$$

The material horizon gradient in the first term on the RHS can be further expanded using the product rule and the definition of the horizon deformation gradient $\boldsymbol{\Phi}^{|} = \partial \boldsymbol{v}^{|} / \partial \boldsymbol{\Xi}^{|}$ in Eq. (30) as

$$\nabla_{\Xi^{|}} \left(w_0^{|} \, \Xi^{|} \right) = \partial_{\lambda^{|}} w_0^{|} \left[\boldsymbol{e}^{|} \cdot \boldsymbol{\Phi}^{|} - \lambda^{|} \, \boldsymbol{E}^{|} \right] + w_0^{|} \, \boldsymbol{E}^{|} \,. \tag{49}$$

Observing that $\boldsymbol{p}^{|}$ as defined in Eq. (37) is contained in the first term, expressing the second term with the neighbour-wise spatial secant map $\mathbb{F}$ in Eq. (25) and then recognising the energy–momentum format of the bond-wise Eshelby-type interaction force $\boldsymbol{S}^{|}$ in Eq. (45), the material horizon gradient of the bond-wise potential energy is finally given by

$$\nabla_{\Xi^{|}} \left(w_0^{|} \, \Xi^{|} \right) = \boldsymbol{p}^{|} \cdot \boldsymbol{\Phi}^{|} - \mathbb{F}^{\mathrm{t}} \cdot \boldsymbol{p}^{|} + w_0^{|} \, \boldsymbol{E}^{|} = \boldsymbol{p}^{|} \cdot \boldsymbol{\Phi}^{|} + \boldsymbol{S}^{|} \,. \tag{50}$$

Substituting this result back into Eq. (47) renders

$$\begin{aligned} \int_{\mathcal{N}_0} \boldsymbol{S}^{|} \, \mathrm{d}N^{|} &= - \int_{\mathcal{N}_0} \boldsymbol{p}^{|} \cdot \boldsymbol{\Phi}^{|} \, \mathrm{d}N^{|} \\ &= -\boldsymbol{F}^{\mathrm{t}} \cdot \int_{\mathcal{N}_0} \boldsymbol{p}^{|} \, \mathrm{d}N^{|} - \left[\frac{1}{1!} \int_{\mathcal{N}_0} \boldsymbol{p}^{|} \otimes \boldsymbol{\Xi}^{|} \, \mathrm{d}N^{|} : \nabla_{\boldsymbol{X}} \boldsymbol{F} \right. \\ &\quad \left. + \frac{1}{2!} \int_{\mathcal{N}_0} \boldsymbol{p}^{|} \otimes \boldsymbol{\Xi}^{|} \otimes \boldsymbol{\Xi}^{|} \, \mathrm{d}N^{|} \cdot : \nabla_{\boldsymbol{X}}^2 \boldsymbol{F} + \cdots \right] \\ &=: -\boldsymbol{F}^{\mathrm{t}} \cdot \int_{\mathcal{N}_0} \boldsymbol{p}^{|} \, \mathrm{d}N^{|} - \boldsymbol{B}_0^{\odot} \,. \end{aligned} \tag{51}$$

Observe that the first term on the right-hand side is a local covariant transformation from the spatial to the material point-wise force density, whereas the remaining terms, abbreviated as the material force density $\boldsymbol{B}_0^{\odot}$, capture the contribution of non-locality via higher-order moments of the bond-wise spatial interaction force $\boldsymbol{p}^{|}$ and higher-order deformation gradients $\nabla_{\boldsymbol{X}}^{1,2,\cdots} \boldsymbol{F}$. Collectively, these non-local terms disappear for vanishing horizon size $\delta_0 \to 0$ and/or a point-wise smooth deformation with vanishing higher-order deformation gradients $\nabla_{\boldsymbol{X}}^{1,2,\cdots} \boldsymbol{F} \to \boldsymbol{0}$. The non-local material body force density $\boldsymbol{B}_0^{\odot}$ arises from non-locality due to the integrals over the horizon and is thus different from the material inhomogeneity force density $\boldsymbol{B}_0$ in CCM that occurs due to the dependence of the potential energy density on the material placement $\boldsymbol{X}$. In PD an additional material inhomogeneity force density would arise if the current assumption on the homogeneity of the bond-wise potential energy $w_0^{|} \neq w_0^{|}(\boldsymbol{\Xi}^{|})$ were relaxed.

In the same manner that the localised force balances in the different settings in CCM are related through Piola transforms and pull-back/push-forward operations (see Fig. 2), the point-wise force balances in the different settings in PD can also be related through suitable Piola transforms (reducing here to a scaling by the Jacobian) and covariant pull-back/push-forward operations, i.e., by the transposed local deformation gradient (see Fig. 7). Most of the contributions on PD are formulated in a Lagrangian framework, with a few recent works that investigate the updated Lagrangian or Eulerian approaches, see for example (Bergel and Li, 2016; Behzadinasab and Foster, 2020; Silling et al., 2017; Menon and Song, 2022). One of the key features of this contribution is that it provides a unifying approach to consistently relate the point-wise force balances in Lagrangian and Eulerian settings.

Finally, the energy release in Eq. (40) is rewritten as

$$\mathcal{R} := - \int_{\mathcal{B}_0} \int_{\mathcal{N}_0} \boldsymbol{S}^{|} \, \mathrm{d}N^{|} \cdot \mathrm{d}_{\delta} \boldsymbol{Y} \, \mathrm{d}V = \int_{\mathcal{B}_0} \boldsymbol{B}_0^{\odot} \cdot \mathrm{d}_{\delta} \boldsymbol{Y} \, \mathrm{d}V \leq 0 \,. \tag{52}$$

In contrast to CCM the energy release in PD is due to the non-local force density $\boldsymbol{B}_0^{\odot}$, which stems from the non-local pull-back operation acting on $\boldsymbol{p}^{|}$ (Eq. $(51)_1$). The non-local material force density $\boldsymbol{B}_0^{\odot}$ vanishes in the local limit $\delta_0 \to 0$, while retaining localised contributions at boundaries and interfaces as in CCM.

Remark 7. In Steinmann et al. (2011, 2021) the relation between the spatial and material atom-wise forces was not explicitly given; however, conceptually its derivation would follow similar steps as in the case of PD with integrals substituted by summations. The procedure will be detailed in a separate contribution. □

3.4. Energy release at a crack tip

When considering a crack tip, the corresponding energy release can be determined by considering the contribution of the non-local force

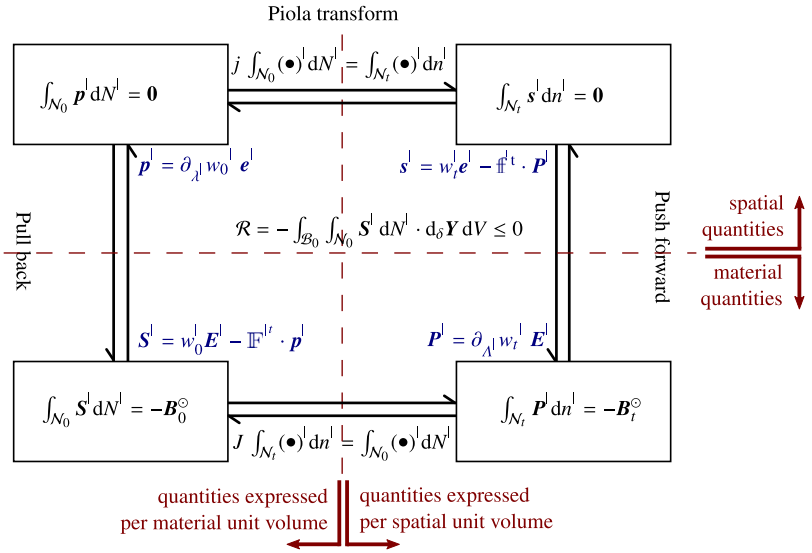

Fig. 7. Transformations between equivalent point-wise force balance equations in PD.

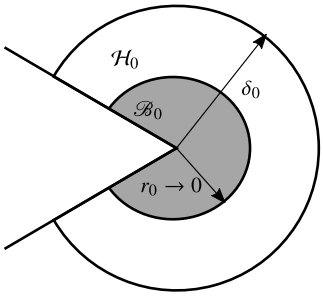

Fig. 8. Crack tips are considered by cutting out a ball $\mathscr{B}_0$ with radius r_0 and letting it tend to zero.

density $\boldsymbol{B}_0^{\odot}$ *within* a ball $\mathscr{B}_0$ with radius r_0 containing the crack tip and letting the radius of the ball shrink to zero, that is

$$\begin{aligned}\mathcal{R}_{\text{crack}} &= -\lim_{r_0 \to 0} \int_{\mathscr{B}_0} \int_{\mathcal{N}_0} \boldsymbol{S}^{\mid} \mathrm{d}N^{\mid} \cdot \mathrm{d}_{\delta} \boldsymbol{Y} \mathrm{d}V \\ &= -\int_{\mathcal{N}_0} \lim_{r_0 \to 0} \int_{\mathscr{B}_0} \boldsymbol{S}^{\mid} \cdot \mathrm{d}_{\delta} \boldsymbol{Y} \mathrm{d}V \mathrm{d}N^{\mid} \\ &= -\int_{\mathcal{N}_0} \boldsymbol{S}^{\mid}\big|_{r_0=0} \mathrm{d}N^{\mid} \cdot \mathrm{d}_{\delta} \boldsymbol{Y}\big|_{r_0=0} \\ &:= -\int_{\mathcal{N}_0} \boldsymbol{J}^{\mid} \mathrm{d}N^{\mid} \cdot \mathrm{d}_{\delta} \boldsymbol{Y}\big|_{r_0=0} = -\boldsymbol{J}^{\odot} \cdot \mathrm{d}_{\delta} \boldsymbol{Y}\big|_{r_0=0}.\end{aligned} \tag{53}$$

Here $\boldsymbol{J}^{\mid} := \boldsymbol{S}^{\mid}\big|_{r_0=0}$ refers to a neighbour-wise measure analogous to the vectorial $\boldsymbol{J}$ from classical fracture mechanics. The point-wise measure $\boldsymbol{J}^{\odot} := \int_{\mathcal{N}_0} \boldsymbol{J}^{\mid} \mathrm{d}N^{\mid}$ corresponds to the vectorial version of the J-integral from classical fracture mechanics and should be compared to Eq. $(11)_b$

$$\boldsymbol{J}^{\odot} =: \int_{\mathcal{N}_0} \boldsymbol{S}^{\mid}\big|_{r_0=0} \mathrm{d}N^{\mid} =: \int_{\mathcal{N}_0} \boldsymbol{J}^{\mid} \mathrm{d}N^{\mid}. \tag{54}$$

Here the non-locality stems from the fact that even though we let the ball $\mathscr{B}_0$ shrink to zero, the size of the neighbourhood remains unchanged, i.e., there are contributions from all the neighbours within $\mathcal{H}_0$ (see Fig. 8).

4. What can peridynamic configurational forces tell us?

The purpose of this section is to elucidate the theory developed through a computational example, which, for the sake of demonstration, is restricted to two dimensions. These are devised to highlight key features of configurational forces in PD. The pertinent results are contrasted to their counterparts in CCM as obtained via the finite element method (FEM). To this end, to allow for meaningful comparison, bi-linear finite elements are used for CCM with their edge size equal to the grid-spacing L of the PD computations. The computational domain is a unit square with a square hole at its centre, with an edge size of 0.4. A uniform expansion of 1% is imposed via Dirichlet-type boundary conditions on the outer boundary of the unit square. The resulting configurational forces within the domain, and in particular at the corners of the square hole, are computed and assessed. For PD, additional boundary layers, with size proportional to δ_0/L, are introduced in order to prescribe the displacement boundary conditions. The domain is discretised with 20, 40, 100 and 200 divisions per side. For PD, this gives grid points with $L = 0.05$, $L = 0.025$, $L = 0.01$ and $L = 0.005$, respectively, see Fig. 9. For the PD simulations $\delta_0/L \approx 3$. This gives the same number of integration points within the horizon, hence the same numerical accuracy for the calculations within the horizon. With δ_0/L fixed, the influence of non-locality is studied by varying the grid-spacing L as a smaller L implies a more local material behaviour. The FEM simulations do not show a significant difference when the number of elements is varied. This is expected as CCM is a local formulation. By contrast, the PD simulations demonstrate the non-local attributes of the underlying model with configurational forces arising both on the boundary and in the interior of the domain. The latter is absent in the FEM simulations of CCM.

The constitutive behaviour in CCM follows the model of classical neo-Hookean hyper-elasticity with the potential energy density U_0 per volume in the material configurational given by

$$\begin{aligned}U_0 &= \tfrac{1}{2}\mu\,[\boldsymbol{F} : \boldsymbol{F} - 2 - 2\log J] \\ &\quad + \tfrac{1}{2}\lambda\,\big[\tfrac{1}{2}\,[J^2 - 1] - \log J\big] \qquad \text{with} \qquad J := \mathrm{Det}\boldsymbol{F}\,,\end{aligned} \tag{55}$$

where λ and μ are the first and second Lamé parameters, respectively. To allow for direct comparison with bond-based PD in 2D, the material parameters for CCM are selected to be $\mu = \lambda = 100$ so as to recover a Poisson ratio of $\nu = 1/3$. Note that the term 2D here refers to a

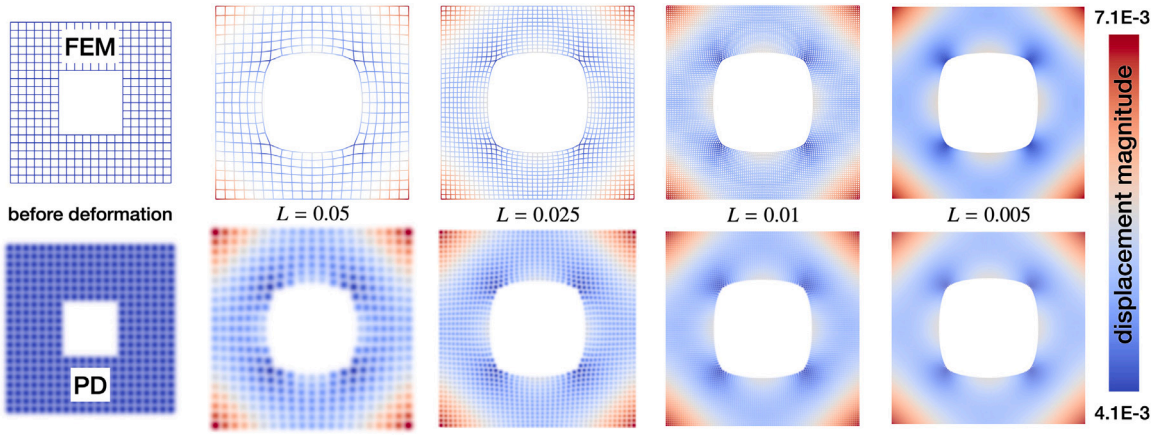

Fig. 9. The discretisation and deformation of the unit square domain with a hole under an expansion of 1% prescribed on its external boundary. The deformation is magnified 20 times. Bi-linear finite elements are employed for FEM with their edge size equal to the grid-spacing L of PD computations. The blur on the PD results is artificially added, for the sake of a better illustration of the region as a continuous domain.

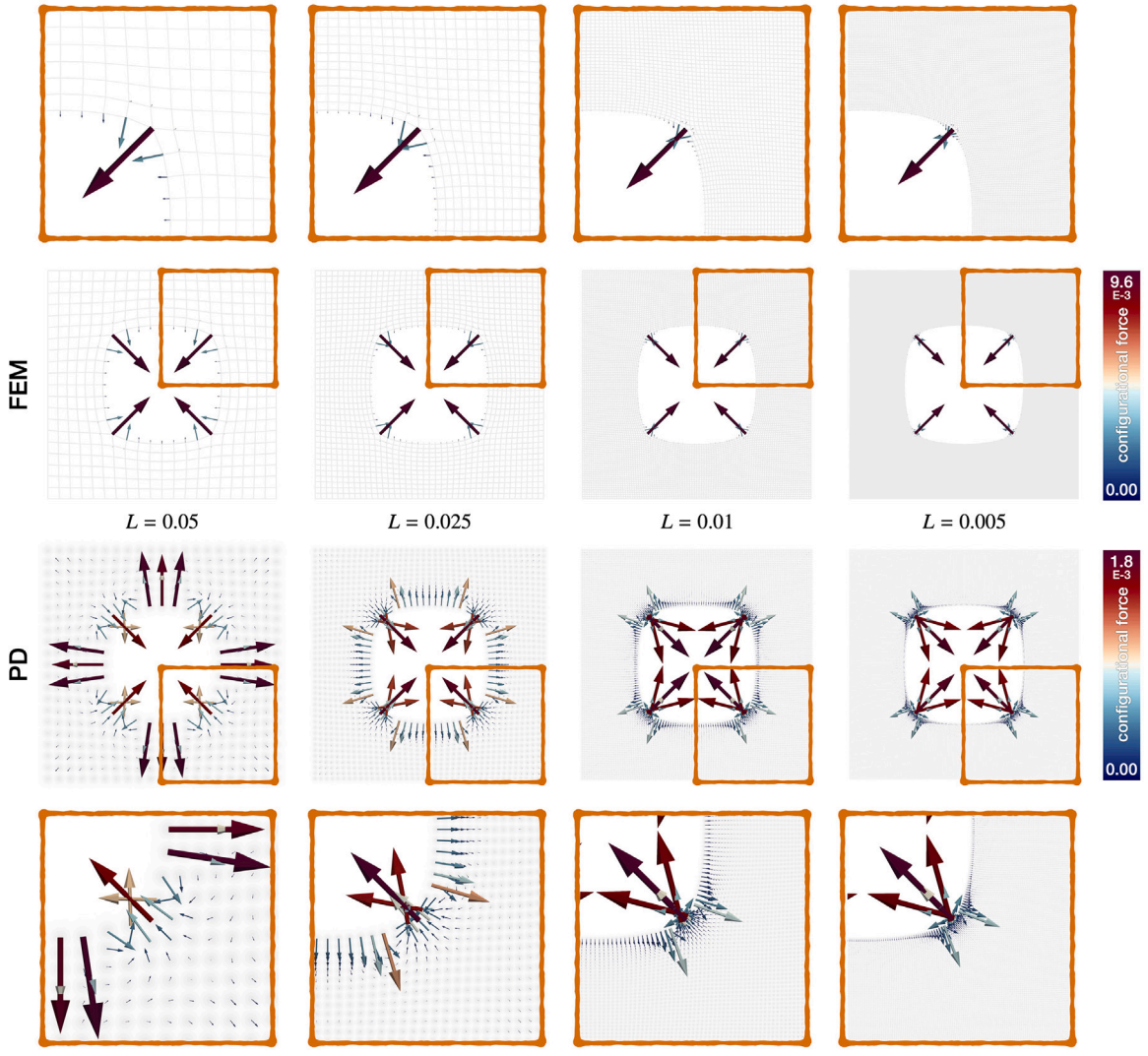

Fig. 10. The deformation of the unit square domain with a hole under an expansion of 1% prescribed on its external boundary, magnified 20 times. The arrows indicate the configurational forces for FEM in the first row and for PD in the second row. The four columns correspond to the PD grid-spacing $L = 0.05$, $L = 0.025$, $L = 0.01$ and $L = 0.005$ from left to right and FEM computations employ bi-linear elements associated with the discretisation of their PD counterparts. For PD simulations δ_0/L is fixed resulting in higher non-locality when increasing the grid-spacing L. The configurational forces in FEM are nearly independent of the discretisation. However, for PD computations, via decreasing L and thus $\delta_0 \approx 3L$ from left to right, the non-locality decreases and the corresponding configurational forces are affected.

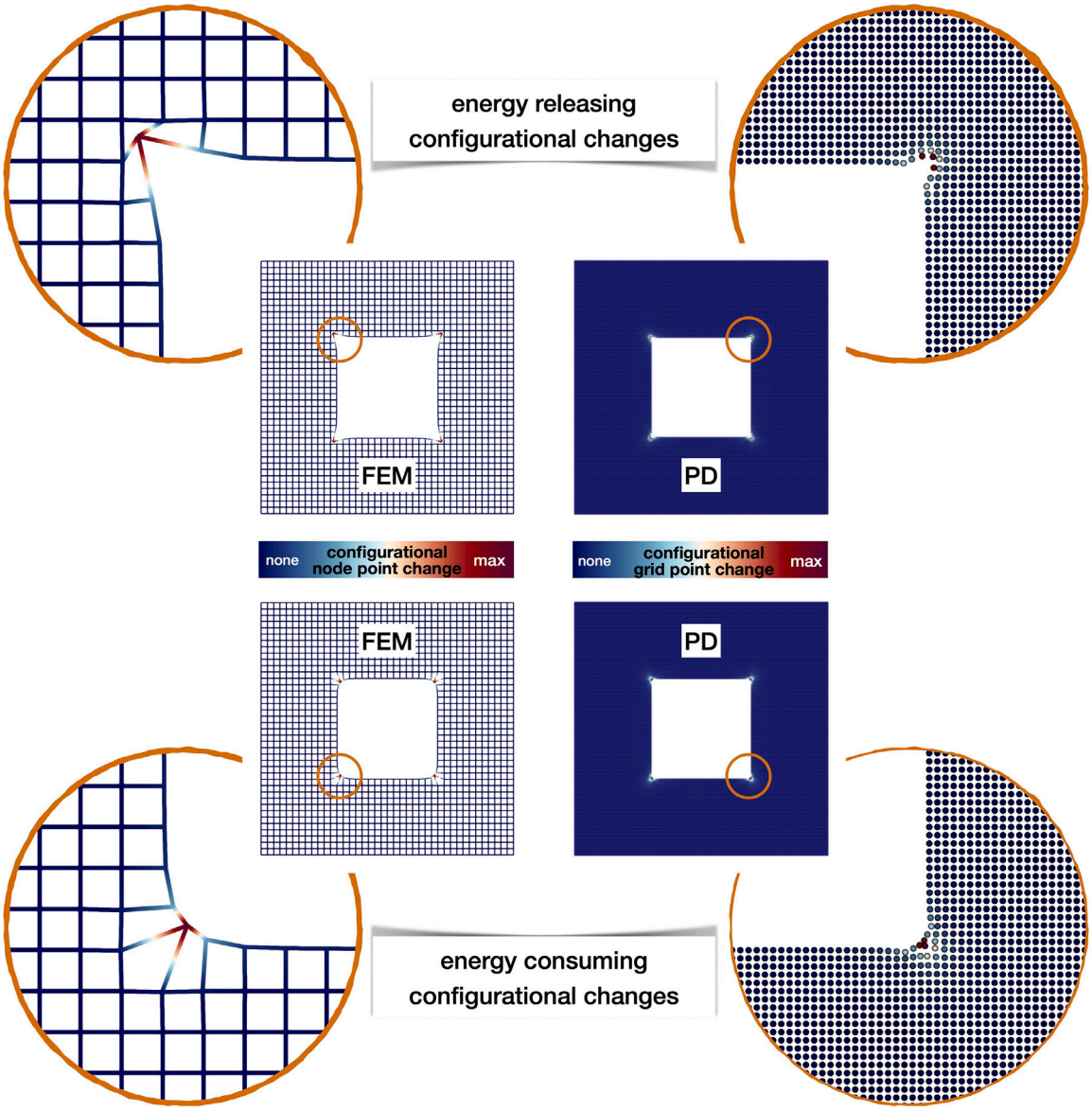

Fig. 11. Energetically favoured configurational changes of the domain for FEM (left) and PD (right). In order to obtain these results, the reference domains are modified either positively or negatively proportional to the configurational force vectors. The magnitude of the change in FEM is five times larger than its PD counterparts.

truly two-dimensional manifold in a two-dimensional space reminiscent of surface elasticity theory, i.e., it is neither the degenerate three-dimensional cases of plane-stress nor plane-strain. The neighbour-wise bond energy density $w_0^{|}$ per length $\Xi^{|}$ in the material configuration is chosen to be a harmonic function given by

$$w_0^{|} = \tfrac{1}{2}\, C^{|}\, [\lambda^{|} - 1]^2 \qquad \text{with} \qquad \lambda^{|} := \frac{v^{|}}{\Xi^{|}}\,, \tag{56}$$

where $C^{|}$ is the neighbour-wise stiffness coefficient. Under infinitesimal affine deformations, the energy density of CCM and PD match resulting in the following relationships between their material parameters (see Ekiz et al., 2022):

$$C^{|} = \frac{24}{\pi\, \delta_0^3}\mu \qquad \Leftrightarrow \qquad \mu = \lambda = \frac{\pi\, \delta_0^3}{24} C^{|}\,. \tag{57}$$

All the numerical examples are configured to exhibit small deformations such that both CCM and PD will follow a near-linear material response to aid comparison.

Fig. 10 shows the distribution of configurational forces within the domain for each discretisation together with a magnified version of a quarter of the domain in each case. The numerical results show clearly that the distribution of configurational forces in FEM is almost independent of the mesh size. Here the configurational forces are concentrated at the corners and nearly vanish completely within the domain, consistent with $\boldsymbol{B}_0 = \boldsymbol{0}$. For PD, the configurational forces in the domain correspond to $\boldsymbol{B}_0^{\odot}$ which capture the contribution of non-locality via higher-order moments of $\boldsymbol{p}^{|}$ and higher deformation gradients. The PD computations differ further from those of FEM as the discretisation of the domain impacts the results. The reason for this is that the PD computations here have a fixed δ_0/L. A larger L therefore naturally results in a proportionally larger δ_0 which consequently increases the degree of non-locality. Furthermore, the largest magnitude of the configurational forces in PD are *individually* significantly smaller than their FEM counterparts. However, their sum agrees with that of FEM as the horizon size goes to zero. This is simply due to the non-locality of the PD computations in the sense that the classical concentration due to the "corner effect" is far less pronounced in the

case of PD as compared to FEM. Obviously, non-localities are absent in these FEM computations and therefore, the results in the upper half are more self-similar compared to their PD counterparts in the lower half. Finally, for illustrative purposes, in Fig. 11 we modify the reference domain either positively or negatively proportional to the configurational force vectors to capture the *energetically favoured* configurational changes so as to either release or consume energy upon configurational changes. Both FEM and PD computations predict similar configurational changes, especially near the corners.

The example could be modified to have a rigid inclusion rather than a void in the centre. It is expected that for this extension the configurational force would act in the opposite direction to that shown here, as known from J-integral/energy release rate considerations for rigid inclusion problems in elasticity (Wang et al., 1985; Bigoni et al., 2008).

5. Summary and outlook

PD is a non-local continuum formulation combining concepts from both atomistic and continuum mechanics. It is characterised by the absence of spatial derivatives in the expression of the point-wise internal force density that results from an integration over the horizon rather than from the divergence of a stress measure. Being free from spatial derivatives has made PD popular for problems involving initiation and propagation of discontinuities, such as cracks. This perception is however somewhat deceptive since apparent crack initiation and subsequent propagation in PD is due to a constitutive prescription allowing the bond-wise interaction forces to decay with increasing elongation of the bonds. Thus, as in atomistic mechanics, without further artificial criteria for bond deletion, classical PD does not include irreversibility or dissipation upon crack initiation and propagation and, therefore, can at best describe monotonic loading situations. This situation is not dissimilar to phase field modelling of cracks that also requires additional irreversibility criteria to give it the flavour of a gradient damage formulation. Our rational, and the motivation for the work that has been presented, is that in a continuum body i) initiation of a true crack always comes with an alteration of the topology describing the geometry of the body, and (ii) propagation of a true crack is irreversible and comes with energy dissipation in the body, or, differently expressed, energy release from the body. These important aspects of crack initiation and propagation are jointly captured by configurational changes, a notion that has been entirely absent in treatments of PD to date.

This contribution addresses these deficiencies by laying the groundwork for a rigorous formulation of configurational peridynamics. To reconcile further the summation over neighbours in discrete atomistic systems with the integration over the horizon in PD, the novel concept of bond number double-density has been introduced. Using this concept, spatial and material variations of the potential energy functional result in the quasi-static localised force balances in spatial and material setting. Interestingly, these can be related by non-local pull-back and push-forward operations that degenerate in the local limit to the common covariant transformation with the deformation gradient of local continuum mechanics. Our approach allows one to distinguish, for the first time, between Piola-type and Cauchy-type versions of the common bond-wise (spatial) interaction forces. Moreover, our approach has introduced novel Piola-type and Cauchy-type versions of bond-wise material interaction forces; remarkably, the latter in an Eshelby-type energy–momentum format. Their horizon integral equilibrates with the point-wise material body force density arising due to non-locality. The non-local material body force density is directly responsible for the energy release (or consumption) upon configurational changes in a PD continuum. For the geometrically limiting case of a crack tip, a true PD version of the celebrated J-integral of fracture mechanics taking into account the non-locality of PD follows as the horizon integral of the bond-wise material interaction forces evaluated at the crack tip.

This work provides the necessary configurational framework (toolbox) to consider true cracks in PD with topology altering crack initiation and irreversible, i.e., dissipative, crack propagation. Our illustration of the implications of configurational PD for a two-dimensional problem with singular geometry clearly demonstrates that the computationally determined configurational forces in PD vary with the degree of non-locality and can be used to determine, in a rational way, either energy releasing or energy consuming configurational changes. We are thus convinced that configurational peridynamics holds great promise for treating problems with configurational changes such as true cracks and other topology altering defects in a PD continuum.

In our forthcoming work we will extend the present configurational peridynamics framework to the case of Continuum-Kinematics-Inspired PD (CPD), i.e., from the here considered case of one neighbour interactions to the general case including also two and three neighbour interactions.

Declaration of competing interest

The authors declare that they have no known competing financial interests or personal relationships that could have appeared to influence the work reported in this paper.

Data availability

No data was used for the research described in the article.

Acknowledgements

PS and AMcB acknowledge support from the UK Engineering and Physical Sciences Research Council grant EP/R008531/1 for the Glasgow Computational Engineering Centre. PS acknowledges support from the European Research Council (ERC) under the Horizon Europe programme (Grant-No. 101052785, project: SoftFrac) and by the Deutsche Forschungsgemeinschaft, Germany (DFG, German Research Foundation) - 377472739/GRK 2423/1-2019. AdV acknowledges support from the National Research Foundation of South Africa (Grant number 121926). AJ gratefully acknowledges the support provided by the Scientific and Technological Research Council of Turkey (TÜBITAK) Career Development Program, grant number 218M700. The final version of the manuscript has been seen and approved by all authors. It is the author's original work, has not received prior publication and is not under consideration for publication elsewhere.

References

Armanini, C., Dal Corso, F., Misseroni, D., Bigoni, D., 2019. Configurational forces and nonlinear structural dynamics. J. Mech. Phys. Solids 130, 82–100.

Behzadinasab, M., Foster, J.T., 2020. A semi-Lagrangian constitutive correspondence framework for peridynamics. J. Mech. Phys. Solids 137, 103862.

Bergel, G.L., Li, S., 2016. The total and updated Lagrangian formulations of state-based peridynamics. Comput. Mech. 58 (2), 351–370.

Bigoni, D., Dal Corso, F., Gei, M., 2008. The stress concentration near a rigid line inclusion in a prestressed, elastic material. Part II.: Implications on shear band nucleation, growth and energy release rate. J. Mech. Phys. Solids 56 (3), 839–857.

Bobaru, F., Zhang, G., 2015. Why do cracks branch? A peridynamic investigation of dynamic brittle fracture. Int. J. Fract. 196 (1–2), 59–98.

Bosi, F., Misseroni, D., Dal Corso, F., Neukirch, S., Bigoni, D., 2016. Asymptotic self-restabilization of a continuous elastic structure. Phys. Rev. E 94 (6), 063005.

Butt, S.N., Meschke, G., 2021. Peridynamic analysis of dynamic fracture: influence of peridynamic horizon, dimensionality and specimen size. Comput. Mech. 67 (6), 1719–1745.

Cermelli, P., Fried, E., 1997. The influence of inertia on the configurational forces in a deformable solid. Proc. R. Soc. Lond. Ser. A Math. Phys. Eng. 453, 1915–1927.

Cermelli, P., Fried, E., Sellers, S., 2001. Configurational stress, yield and flow in rate–independent plasticity. Proc. R. Soc. Lond. Ser. A Math. Phys. Eng. Sci. 457 (2010), 1447–1467.

Cordero, N.M., Forest, S., Busso, E.P., 2016. Second strain gradient elasticity of nano-objects. J. Mech. Phys. Solids 97, 92–124.

Dell'Isola, F., Andreaus, U., Placidi, L., 2015. At the origins and in the vanguard of peridynamics, non-local and higher-gradient continuum mechanics: An underestimated and still topical contribution of Gabrio Piola. Math. Mech. Solids 20 (8), 887–928.

Dillard, T., Forest, S., Ienny, P., 2006. Micromorphic continuum modelling of the deformation and fracture behaviour of nickel foams. Eur. J. Mech. A 25 (3), 526–549.

Dorduncu, M., Madenci, E., 2022. Finite element implementation of ordinary state-based peridynamics with variable horizon. Eng. Comput. http://dx.doi.org/10.1007/s00366-022-01641-6.

Ebrahimi, S., Steigmann, D., Komvopoulos, K., 2015. Peridynamics analysis of the nanoscale friction and wear properties of amorphous carbon thin films. J. Mech. Mater. Struct. 10, 559–572.

Ekiz, E., Steinmann, P., Javili, A., 2022. Relationships between the material parameters of continuum-kinematics-inspired peridynamics and isotropic linear elasticity for two-dimensional problems. Int. J. Solids Struct. 238, 111366.

Eshelby, J.D., 1951. The force on an elastic singularity. Proc. R. Soc. A 244 (877), 87–112.

Eshelby, J., 1975. The elastic energy-momentum tensor. J. Elasticity 5 (3–4), 321–335.

Forest, S., 2009. Micromorphic approach for gradient elasticity, viscoplasticity, and damage. J. Eng. Mech. 135 (3), 117–131.

Fried, E., 2010. New insights into the classical mechanics of particle systems. Discrete Contin. Dyn. Syst. 28 (4), 1469–1504.

Fried, E., Gurtin, M.E., 2003. The role of the configurational force balance in the nonequilibrium epitaxy of films. J. Mech. Phys. Solids 51, 487–517.

Gurtin, M.E., 1995. The nature of configurational forces. Arch. Ration. Mech. Anal. 131 (1), 67–100.

Gurtin, M.E., 2000. Configurational Forces as Basic Concepts of Continuum. Springer.

Gurtin, M.E., Podio-Guidugli, P., 1996a. Configurational forces and the basic laws for crack propagation. J. Mech. Phys. Solids 44 (6), 905–927.

Gurtin, M.E., Podio-Guidugli, P., 1996b. On configurational inertial forces at a phase interface. J. Elasticity 44 (3), 255–269.

Gurtin, M.E., Podio-Guidugli, P., 1998. Configurational forces and a consititutive theory for crack propagation that allows for kinking and curving. J. Mech. Phys. Solids 46 (8), 1343–1378.

Ha, Y.D., Bobaru, F., 2011. Characteristics of dynamic brittle fracture captured with peridynamics. Eng. Fract. Mech. 78 (6), 1156–1168.

Javili, A., McBride, A., Steinmann, P., 2019a. Continuum-kinematics-inspired peridynamics. Mechanical problems. J. Mech. Phys. Solids 131, 125–146.

Javili, A., Morasata, R., Oterkus, E., Oterkus, S., 2019b. Peridynamics review. Math. Mech. Solids 24, 3714–3739.

Kienzler, R., Herrmann, G., 2000. Mechanics in Material Space: with Applications to Defect and Fracture Mechanics. Springer Science & Business Media.

Kuhn, C., Müller, R., 2016. A discussion of fracture mechanisms in heterogeneous materials by means of configurational forces in a phase field fracture model. Comput. Methods Appl. Mech. Engrg. 312, 95–116.

Liakou, A., Detournay, E., 2018. Constrained buckling of variable length elastica: Solution by geometrical segmentation. Int. J. Non-Linear Mech. 99, 204–217.

Maugin, G.A., 1995. Material forces: Concepts and applications. Appl. Mech. Rev. 48 (5), 213–245.

Maugin, G.A., 2016. Configurational Forces: Thermomechanics, Physics, Mathematics, and Numerics. CRC Press.

Maugin, G.A., 2020. Material Inhomogeneities in Elasticity. CRC Press.

Menon, S., Song, X., 2022. Updated Lagrangian unsaturated periporomechanics for extreme large deformation in unsaturated porous media. Comput. Methods Appl. Mech. Engrg. 400, 115511.

Näser, B., Kaliske, M., Müller, R., 2007. Material forces for inelastic models at large strains: Application to fracture mechanics. Comput. Mech. 40 (6), 1005–1013.

Podio-Guidugli, P., 2002. Configurational forces: are they needed? Mech. Res. Commun. 29 (6), 513–519.

Silling, S.A., 2000. Reformulation of elasticity theory for discontinuities and long-range forces. J. Mech. Phys. Solids 48 (1), 175–209.

Silling, S., Askari, E., 2005. A meshfree method based on the peridynamic model of solid mechanics. Comput. Struct. 83 (17–18), 1526–1535.

Silling, S.A., Parks, M.L., Kamm, J.R., Weckner, O., Rassaian, M., 2017. Modeling shockwaves and impact phenomena with Eulerian peridynamics. Int. J. Impact Eng. 107, 47–57.

Silling, S.A., Weckner, O., Askari, E., Bobaru, F., 2010. Crack nucleation in a peridynamic solid. Int. J. Fract. 162 (1–2), 219–227.

Steinmann, P., 2002a. On spatial and material settings of hyperelastodynamics. Acta Mech. 156 (3–4), 193–218.

Steinmann, P., 2002b. On spatial and material settings of hyperelastostatic crystal defects. J. Mech. Phys. Solids 50 (8), 1743–1766.

Steinmann, P., 2002c. On spatial and material settings of thermo-hyperelastodynamics. J. Elasticity 66 (2), 109–157.

Steinmann, P., 2008. On boundary potential energies in deformational and configurational mechanics. J. Mech. Phys. Solids 56 (3), 772–800.

Steinmann, P., 2022. Spatial and Material Forces in Nonlinear Continuum Mechanics. Springer.

Steinmann, P., Maugin, G.A., 2006. Mechanics of Material Forces, Vol. 11. Springer.

Steinmann, P., McBride, A., Bargmann, S., Javili, A., 2012. A deformational and configurational framework for geometrically non-linear continuum thermomechanics coupled to diffusion. Int. J. Non-Linear Mech. 47 (2), 215–227.

Steinmann, P., Ricker, S., Aifantis, E., 2011. Unconstrained and Cauchy-Born-constrained atomistic systems: deformational and configurational mechanics. Arch. Appl. Mech. 81 (5), 669–684.

Steinmann, P., Smith, A., Birang, E., McBride, A., Javili, A., 2021. Atomistic two-, three-and four-body potentials. Spatial and material settings. J. Mech. Phys. Solids 154, 104507.

Svendsen, B., Neff, P., Menzel, A., 2009. On constitutive and configurational aspects of models for gradient continua with microstructure. J. Appl. Math. Mech. 89 (8), 687–697.

Wang, Z., Zhang, H., Chou, Y., 1985. Characteristics of the elastic field of a rigid line inhomogeneity. J. Appl. Mech. 52 (4), 818–822.